SECURITY CLASSIFICATION OF THIS PAGE

REPORT DOCUMENTATION PAGE

Form Approved OMB No. 0704-0188

1a. REPORT SECURITY CLASSIFICATION: UNCLASSIFIED	1b. RESTRICTIVE MARKINGS: NONE
2a. [illegible]	3. DISTRIBUTION/AVAILABILITY OF REPORT: APPROVED FOR PUBLIC RELEASE; DISTRIBUTION UNLIMITED.
2b.	
4. P AD-A218 180	5. MONITORING ORGANIZATION REPORT NUMBER(S): AFIT/CI/CIA-89-018
6a. NAME OF PERFORMING ORGANIZATION: AFIT STUDENT AT SAINT LOUIS UNIVERSITY; 6b. OFFICE SYMBOL (If applicable)	7a. NAME OF MONITORING ORGANIZATION: AFIT/CIA
6c. ADDRESS (City, State, and ZIP Code)	7b. ADDRESS (City, State, and ZIP Code): Wright-Patterson AFB OH 45433-6583
8a. NAME OF FUNDING/SPONSORING ORGANIZATION; 8b. OFFICE SYMBOL (If applicable)	9. PROCUREMENT INSTRUMENT IDENTIFICATION NUMBER
8c. ADDRESS (City, State, and ZIP Code)	10. SOURCE OF FUNDING NUMBERS: PROGRAM ELEMENT NO. / PROJECT NO. / TASK NO / WORK UNIT ACCESSION NO.

11. TITLE (Include Security Classification) (UNCLASSIFIED)
A Sub-Cloud Layer Vorticity Budget Analysis for Two Microburst-Producing Storms From Jaws Dual-Doppler Data

12. PERSONAL AUTHOR(S)
Paul G. Lapointe, B.S.

13a. TYPE OF REPORT	13b. TIME COVERED	14. DATE OF REPORT (Year, Month, Day)	15. PAGE COUNT
THESIS/DISSERTATION	FROM _____ TO _____	1989	89

16. SUPPLEMENTARY NOTATION
APPROVED FOR PUBLIC RELEASE IAW AFR 190-1
ERNEST A. HAYGOOD, 1st Lt, USAF
Executive Officer, Civilian Institution Programs

17. COSATI CODES			18. SUBJECT TERMS (Continue on reverse if necessary and identify by block number)
FIELD	GROUP	SUB-GROUP	

19. ABSTRACT (Continue on reverse if necessary and identify by block number)

90 02 14 075

20. DISTRIBUTION/AVAILABILITY OF ABSTRACT	21. ABSTRACT SECURITY CLASSIFICATION
☒ UNCLASSIFIED/UNLIMITED ☐ SAME AS RPT. ☐ DTIC USERS	UNCLASSIFIED

22a. NAME OF RESPONSIBLE INDIVIDUAL	22b. TELEPHONE (Include Area Code)	22c. OFFICE SYMBOL
ERNEST A. HAYGOOD, 1st Lt, USAF	(513) 255-2259	AFIT/CI

DD Form 1473, JUN 86 — Previous editions are obsolete. — SECURITY CLASSIFICATION OF THIS PAGE

AFIT/CI "OVERPRINT"

A SUB-CLOUD LAYER VORTICITY BUDGET ANALYSIS FOR TWO MICROBURST-PRODUCING STORMS FROM JAWS DUAL-DOPPLER DATA

Paul G. Lapointe, B.S.

A Digest Presented to the Faculty of the Graduate School
of Saint Louis University in Partial Fulfillment of
the Requirements for the Degree of
Master of Science (Research)

1989

DIGEST

A vorticity component and budget analysis in three-dimensions is conducted for the subcloud layer of two microburst-producing storms using dual-Doppler derived winds. The raw data were collected during the Joint Airport Weather Studies (JAWS) project. This research examines the vorticity associated with a single microburst-producing storm which occurred on 14 July 1982 and a multiple microburst-producing storm which occurred on 5 August 1982. The calculated vorticity data are examined over the storm domain (10 km x 10 km for the 14 July case and 15 km x 15 km for the 5 August case) and the microburst domain (5 km x 5 km) including two analysis times for the first case and three for the latter case.

Results indicate that horizontal vorticity centers are coincident with strong horizontal gradients of vertical velocity and with areas of strong vertical shear. These gradients are maximized along the edges of downrushing air and along gust fronts. Regions of high speed low-level winds have a core of horizontal vorticity above them.

A vorticity budget analysis of the advection, divergence, and tilting terms, comprising the vorticity component equations, shows the magnitude of these terms to be greater in the microburst domain than in the storm domain. This indicates the strongest forcing and advection takes place within small

regions of the storms. The diverging outflow of the microburst in both cases weakens any existing positive vorticity in the microburst region, e.g., below 0.75 km.

The differences in storm structure allow examination of the vorticity of a simple, nearly circular-symmetric microburst and that of a microburst within a complicated flow field. This leads to different vorticity distributions and budgets.

A SUB-CLOUD LAYER VORTICITY BUDGET ANALYSIS FOR TWO MICROBURST-PRODUCING STORMS FROM JAWS DUAL-DOPPLER DATA

Paul G. Lapointe, B.S.

A Thesis Presented to the Faculty of the Graduate School
of Saint Louis University in Partial Fulfillment of
the Requirements for the Degree of
Master of Science (Research)

1989

COMMITTEE IN CHARGE OF CANDIDACY:

Professor Yeong-jer Lin,
Chairperson and Advisor

Assistant Professor Lawrence Coy

Associate Professor James T. Moore

ACKNOWLEDGEMENTS

The author would like to thank Dr. Yeong-Jer Lin for his guidance and assistance in completing this project. Additional gratitude is extended to Drs. James T. Moore, Lawrence Coy, and Captain (Dr.) John Coover for their helpful comments and suggestions on project improvement. The author is grateful to Ms Sonia Lasher for her assistance with the Figures and Tables used to create this work. This research project reflects many hours the author spent away from his family. For those times, the author extends his humble apology and deep appreciation to his wife, Julie, for her patience and understanding.

TABLE OF CONTENTS

LIST OF TABLES

LIST OF TABLES (CONTINUED)

LIST OF FIGURES

LIST OF FIGURES (CONTINUED)

1. Introduction

The first measurements of airflow associated with microbursts were made with Doppler radar during the 1978 Northern Illinois Meteorological Research on Downbursts (NIMROD) Project. These measurements can only be treated as single Doppler measurements because the large spacing between radars (60 km baseline) and the curvature of the earth caused resolution problems, i.e., obstruction of low-level wind observations by Doppler radars, past 30 km. NIMROD researchers, however, documented 10 microbursts, 5 gust fronts, and two supercells, but again, the main difficulties were in the ground clutter and curvature of the earth.

The Joint Airport Weather Studies (JAWS) program conducted research through the summer of 1982 to determine the fine-scale structure of thunderstorm kinematics in the vicinity of Denver's Stapleton International Airport (Fujita, 1985). The network included a triple Doppler radar (CP-2, CP-3, and CP-4) triangular network (maximum baseline of 28 km), 27 Portable Automated Mesonet (PAM) stations, 1 Low-Level Wind Shear Alerting System (LLWSAS), 2 CO_2 lidar radars, and 5 research aircraft (Figure 1.1).

Fujita's (1985) definition of a downburst as a strong downdraft which induces an outburst of damaging winds on or near the ground expanded as a result of NIMROD to include two

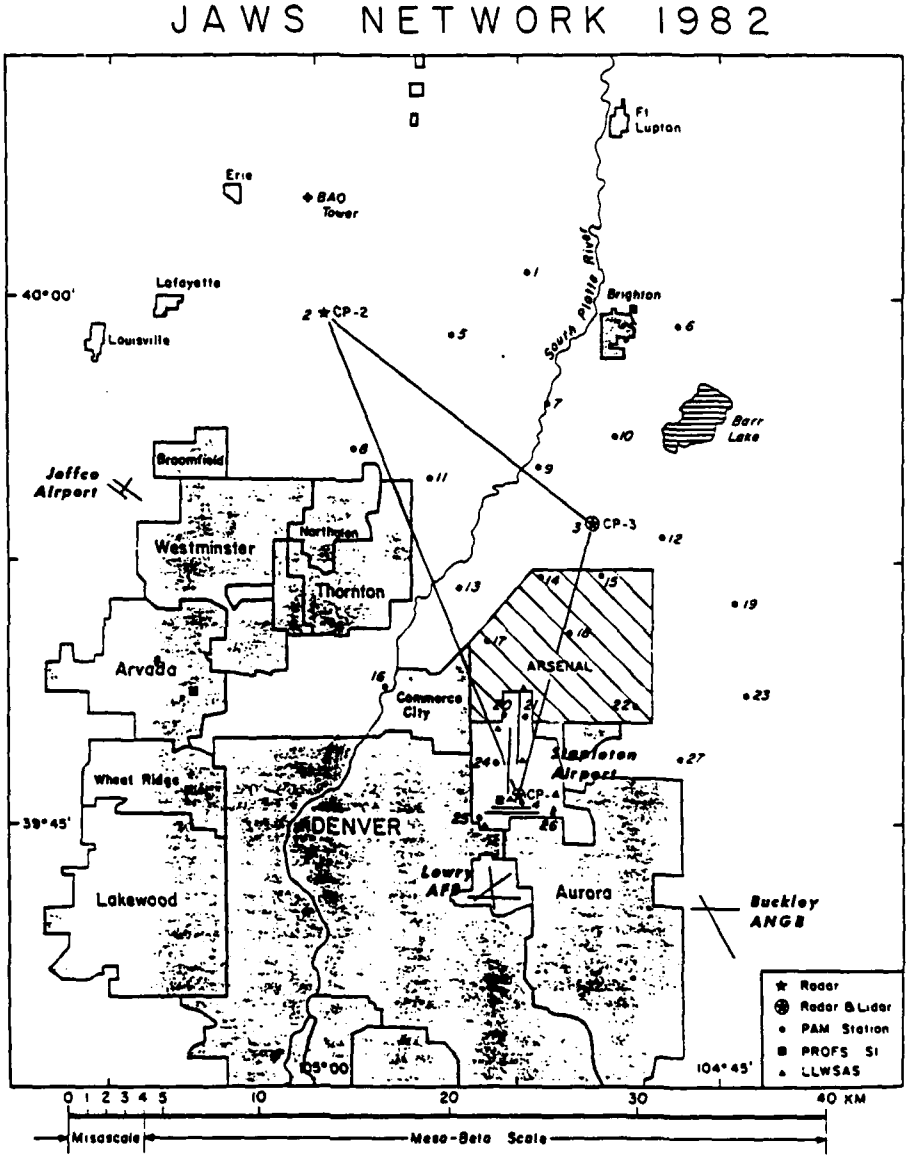

Fig. 1.1: Map illustrating JAWS Project facilities situated in the vicinity of Denver's Stapleton International Airport (after McCarthy et al., 1983).

sub-categories, the macroburst and the microburst. This was to account for the varied length scales of observed downbursts. The microburst, then, became defined as a strong downburst with outflow diameter of less than or equal to 4 km and peak winds lasting 2 to 5 minutes.

Wilson *et al.* (1984) modified Fujita's definition slightly to refer to Doppler radar-observed diverging outflows near the surface associated with convective storms during JAWS. The differential Doppler velocity across the divergence center must be greater than or equal to 10 m/s with initial distance between approaching and receding maximum velocity centers being less than or equal to 4 km. Using this criterion, about 70 microbursts were identified.

These intense, divergent outflows at small scales are considered to be very dangerous to aviation safety. In addition to diverging outflow, horizontal vortices which are common features of microburst outflows (Hjelmfelt, 1987) have been suggested as the cause of 1985 Dallas-Fort Worth L-1011 jet aircraft crash (Fujita, 1986).

Figure 1.2 shows a schematic in the vertical of an evolving microburst wind field (Wilson *et al.*, 1984). Notice at time T-2 minutes the downdraft begins to diverge horizontally and lower to below 1 km with possible horizontal roll vortices developing on the edges of the outflow. With time the vortex

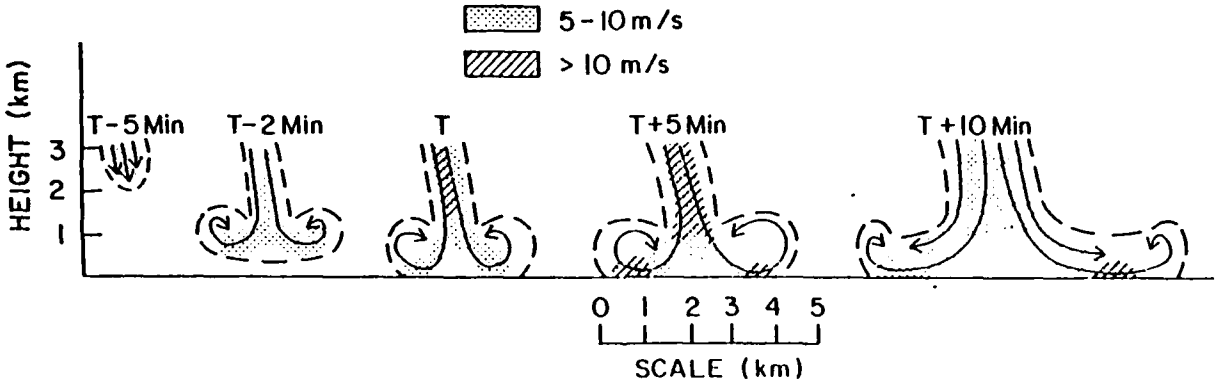

Fig. 1.2: Vertical cross section of the evolution of the microburst wind field based on JAWS data. T is the time of initial divergence at the surface. The shading refers to the vector wind speeds. (From Wilson et al. (1984)).

descends further and the surface winds increase. This figure demonstrates the rapid development and evolution typically found with such events.

Kessinger *et al.* (1988) studied the sub-cloud layer of a multicellular storm in Colorado using multiple Doppler derived winds. Their storm produced misocyclones which are horizontal cyclonic circulation centers with diameters of 2-4 km (Fujita, 1985), downbursts, and horizontal vortex circulations. Many studies have examined the rotation (vorticity) generation as it pertains to the mesocyclones that produce tornadoes. Kessinger *et al.* (1988) found that the misocyclone characteristics, differ from those of mesocyclones by having a vorticity maximum near cloud base instead of at low levels and that the low-level positive vertical vorticity is weakened by the low-level divergence associated with the microburst. They also point out that horizontal vortex circulations (rotors) form along the edge of these misocyclones and storm downdrafts and propagate away from the storm. These rotors have also been associated with the regions of maximum surface winds.

The importance of the rotor in causing damage as well as being an aviation hazard has recently come under more study. The rotor core from the microburst outflows has been associated with lower pressure than its surroundings, which acts to accelerate the surface winds (Waranauskas, 1985) leading to an explanation for burst swath damage and why surface wind speeds are greater than the microburst downflow wind speeds.

Waranauskas (1985) further suggests that the axis of the rotor and the microburst coincide thereby linking the rotor as a cause or enhancement of the microburst. Linden and Simpson (1985) state that the wind shear and downward motion associated with the back of the vortex (rotor) may be responsible for the danger of flying through a microburst. An additional mechanism for intensifying the leading-edge vortex may be the existence of rotation in the descending air.

Despite the importance of the microburst, misocyclones, rotors, etc., few studies have been conducted outside the concern for the vertical component of vorticity. This research will utilize the derived wind fields from dual-Doppler radar data by Lin *et al.* (1987), Lin and Hughes (1987), and Lin and Coover (1988) to study the vorticity (in three dimensions) associated with microburst-producing storms.

2. Statement of Problem

The main objective of this research is to study the vorticity associated with microbursts. Since microbursts have rotation around horizontal (e.g., rotors) and vertical (e.g., misocyclones) axes, a three-dimensional analysis is required.

Therefore, a three-dimensional vorticity budget analysis for the subcloud layer of two microburst-producing storms will be examined using wind fields derived from JAWS dual-Doppler radar data. The three-dimensional vorticity equation (Appendix) in vector form will be separated into its three scalar component equations. The specific terms being investigated are the: 1) horizontal advection; 2) vertical advection; 3) vorticity divergence; and 4) tilting terms.

The first storm which occurred on 14 July 1982, produced a single microburst, a rotor, and a gust front. Analysis is performed for 1647 and 1649 MDT. The storm was at its quasi-steady, mature stage at 1647 MDT and began to decay by 1649 MDT. The vorticity vector remained quasi-horizontal through both time periods. Budget information should help determine why no misocyclone was produced in this case.

The second storm, which occurred on 5 August 1982, produced two microbursts, a microburst misocyclone, and a gust front. Analysis is performed for three time periods, 1845, 1847, and 1850 MDT. This storm will allow the study of misocy-

clone evolution.

Finally, a comparison can be made as to the mechanisms responsible for one storm's vorticity field to remain quasi-horizontal while another developed rotation around the vertical axis. The ultimate goal is to understand the importance of the microburst and its associated structure to the generation of vorticity through interpretation of the various terms of those component equations comprising the three-dimensional vorticity equation.

3. Methodology

3.1 Storm Specifics

The three wind components used to conduct this research were derived from dual-Doppler radar data (Lin *et al.*, 1987; Lin and Hughes, 1987; Lin and Coover, 1988). The data were collected in Colorado during JAWS in the summer of 1982. The first case is the 14 July 1982 case (or the simple case) from which a single microburst was produced along with a gust front and horizontal vortex (rotor) circulation (Hughes, 1986; Coover, 1988). This case may be categorized as a quasi-stationary, single microburst event. As such, the specific structure of microburst vorticity can be isolated without contamination from interactions with other microburst outflows. This storm consists of a warm core downburst of air below 0.75 km within an area of moderate reflectivity values. The outflow pattern is nearly circular symmetric. There are two analysis time periods, 1647 and 1649 MDT. At 1647 MDT, both radars were able to scan the entire storm volume (0.25 to 8.5 km), but only data at and below 2 km will be discussed since the 1649 analysis period has no data above this level.

For the 14 July 1982 case, the analysis grid is a 10 km x 10 km grid centered on the microburst with 0.5 km grid spacing in the horizontal and 0.25 km grid spacing in the vertical below 1 km and 0.5 km grid spacing above this level. There-

fore, six levels of the storm are considered at each analysis time. This is the storm domain. A sub-domain or microburst domain has been defined as a 5 km x 5 km horizontal grid centered on the microburst with the same grid spacings as in the storm domain.

The second case is the 5 August 1982 case or complex case which produced two microbursts, a microburst misocyclone, a gust front mesocyclone-like circulation, and gust front (Coover, 1988). In this case, the scan strategy limited the top of the scanned volume to the 1.25 km level. The analysis grid is a 15 km x 15 km grid with a 0.5 km grid spacing horizontally and 0.25 km vertical spacing beginning as with the 14 July case at the 0.25 km level, but for only five levels. The microburst domain is a 5 km x 5 km analysis grid as defined for the 14 July case. Three analysis times are available for the 5 August case; 1845 , 1847, and 1850 MDT.

3.2 Vorticity Analysis

Values for the specific vorticity components, ξ, η, and ζ, were obtained by calculating the shear at each grid point and subtracting the respective values based on the following definitions:

$$\xi = \partial w/\partial y - \partial v/\partial z \; ; \; \eta = \partial u/\partial z - \partial w/\partial x; \qquad \zeta = \partial v/\partial x - \partial u/\partial y. \tag{1}$$

ξ represents rotation in the y-z plane (about the x-axis), η represents rotation in the x-z plane (about the y-axis), and ζ, most commonly used to describe atmospheric circulations, represents rotation in the x-y plane or horizontal plane (about

the z-axis). A positive value for each term is defined as cyclonic rotation about each axis in the positive axis direction using a right-hand Cartesian coordinate system.

In a purely qualitative sense, one would expect significant values of ξ and η in regions of large horizontal gradients of vertical velocity or in regions of strong vertical shear of the horizontal wind, such as those associated with rapidly moving upward or downward flows in thunderstorms or in the lower layers of a microburst. Likewise, the ζ component will be small in divergent flow (irrotational) and large in regions of strong horizontal shear.

The vorticity equation in vector form is obtained by taking the curl of the equation of motion in vector form. Upon recognizing the small effect the rotation of the earth has on the absolute vorticity, 2Ω, at the convective scale, one obtains an expression for the relative (relative to the earth) vorticity vector, $\vec{q}$:

$$\begin{aligned} d\vec{q}/dt &= \partial q/dt + \vec{V}\cdot\vec{\nabla}q + w\partial q/\partial z \\ &= -\vec{q}(\vec{\nabla}_h\cdot\vec{V}_h+\partial w/\partial z) + \vec{q}\cdot\nabla\vec{V} - \vec{\nabla}\times(\alpha\vec{\nabla}P) + \vec{\nabla}\times\vec{F} \end{aligned} \qquad (2)$$

where $\vec{q} = (\hat{i}\xi + \hat{j}\eta + \hat{k}\zeta)$.

Once terms are expanded, grouped, and the correction to the earth relative velocity is made (due to the storm motion), one obtains the vorticity component equations in moving coordinates (following vector dot product operations):

$$\partial\xi/\partial t = -\vec{V}_h \cdot \vec{\nabla}_h \xi - w\partial\xi/\partial z - \xi(\vec{\nabla}_h \cdot \vec{V}_h + \partial w/\partial z) + (\xi\partial u/\partial x + \eta\partial u/\partial y + \zeta\partial u/\partial z)$$
$$-(\partial\alpha/\partial y\partial p/\partial z - \partial\alpha/\partial z\partial p/\partial y) + (\partial f_z/\partial y - \partial f_y/\partial z)$$

$$\partial\eta/\partial t = \underset{(A)}{-\vec{V}_h \cdot \vec{\nabla}_h \eta} \underset{(B)}{- w\partial\eta/\partial z} \underset{(C)}{- \eta(\vec{\nabla}_h \cdot \vec{V}_h + \partial w/\partial z)} + \underset{(D)}{(\xi\partial v/\partial x + \eta\partial v/\partial y + \zeta\partial v/\partial z)}$$
$$\underset{(E)}{-(\partial\alpha/\partial z\partial p/\partial x - \partial\alpha/\partial x\partial p/\partial z)} + \underset{(F)}{(\partial f_x/\partial z - \partial f_z/\partial x)} \qquad (3)$$

$$\partial\zeta/\partial t = -\vec{V}_h \cdot \vec{\nabla}_h \zeta - w\partial\zeta/\partial z - \zeta(\vec{\nabla}_h \cdot \vec{V}_h + \partial w/dz) + (\xi\partial w/\partial x + \eta\partial w/\partial y + \zeta\partial w/\partial z)$$
$$-(\partial\alpha/\partial x\partial p/\partial y - \partial\alpha/\partial y\partial p/\partial x) + (\partial f_y/\partial x - \partial f_x/\partial y)$$

The result is six terms per component equation including: A) horizontal advection; B) vertical advection; C) divergence; D) tilting; E) solenoidal term; and F) friction term. The friction term is generally one order of magnitude smaller than the others and will not be examined here. Likewise, the solenoid term requires retrieved information derived from the recovered winds and is subject to larger uncertainty, hence, it will not be treated here. The other terms can be determined from the three wind components and their spatial derivatives.

A fourth-order finite differencing scheme will be applied in the horizontal and a second-order finite differencing scheme will be used in the vertical to obtain an estimate for each of the remaining terms. The magnitude of these terms can then be determined by taking their respective area means and standard deviations over the domains of interest. The vorticity budget in three directions can be studied using these results.

Therefore, the three component equations of the 3-dimensional vorticity equation used in this research are derived in the Appendix but listed here for convenience:

$$\partial\xi/\partial t = -\vec{\nabla}_h \cdot \vec{\nabla}_h \xi \; -w\partial\xi/\partial z \; -\xi(\vec{\nabla}_h \cdot \vec{\nabla}_h + \partial w/\partial z) \; +(\xi\partial u/\partial x + \eta\partial u/\partial y + \zeta\partial u/\partial z)$$

$$\underset{\text{HAD}}{\partial\eta/\partial t} = \underset{\text{HAD}}{-\vec{\nabla}_h \cdot \vec{\nabla}_h \eta} \; \underset{\text{VAD}}{-w\partial\eta/\partial z} \; \underset{\text{DIV}}{-\eta(\vec{\nabla}_h \cdot \vec{\nabla}_h + \partial w/\partial z)} \; \underset{\text{TILT}}{+(\xi\partial v/\partial x + \eta\partial v/\partial y + \zeta\partial v/\partial z)} \qquad (4)$$

$$\partial\zeta/\partial t = -\vec{\nabla}_h \cdot \vec{\nabla}_h \zeta \; -w\partial\zeta/\partial z \; -\zeta(\vec{\nabla}_h \cdot \vec{\nabla}_h + \partial w/dz) \; +(\xi\partial w/\partial x + \eta\partial w/\partial y + \zeta\partial w/\partial z)$$

HAD is the horizontal advection of the vorticity component in question, while VAD is simply the vertical advection of that quantity. For a given flow in a quasi-steady state flow field, these terms will be largest in the regions of tightest vorticity gradients. DIV represents the generation (positive) of the respective vorticity component through convergence and the last term, TILT represents the generation of vorticity by tilting the vorticity vector into the respective positive axial direction. The solenoidal term and friction terms are not considered here since Lin (1988) showed that friction is one order of magnitude smaller than other terms and the solenoid values are subject to greater uncertainties having been calculated from a derived wind field.

4. Results

4.1 Simple Case: 14 July 1982, 1647 MDT

Figure 4.1 shows the contoured vorticity analysis field for each vorticity component on the horizontal velocity field at the 0.5 km level. The gust front is denoted by the dashed line to the northwest of the center of the microburst, M. The microburst domain is represented by the small box centered on the microburst. ξ has positive values north of the microburst and negative to the south.

The tightest horizontal gradient of ξ appears across the gust front to the northwest, in evidence of the switch in sign of ξ across the front (Fig. 4.1a).

A south to north (S-N on Figure 4.1) crossection of ξ is shown in Figure 4.2a. The gust front is evident (dashed line) from the velocity field north of the microburst. A rotor or horizontal vortex circulation is very apparent in the wind field centered at 0.75 km on the microburst side of the gust front. The ξ field corresponds to a maximum at this location of 18×10^{-3} per second. On the south side of the microburst, the rotor is non-existent although the flow field does show a circulation but it is not closed. Values of ξ are strongly negative here but not as significant as in the rotor to the north. The southern region being on the downwind side of the storm may be the reason the rotation is not as evident.

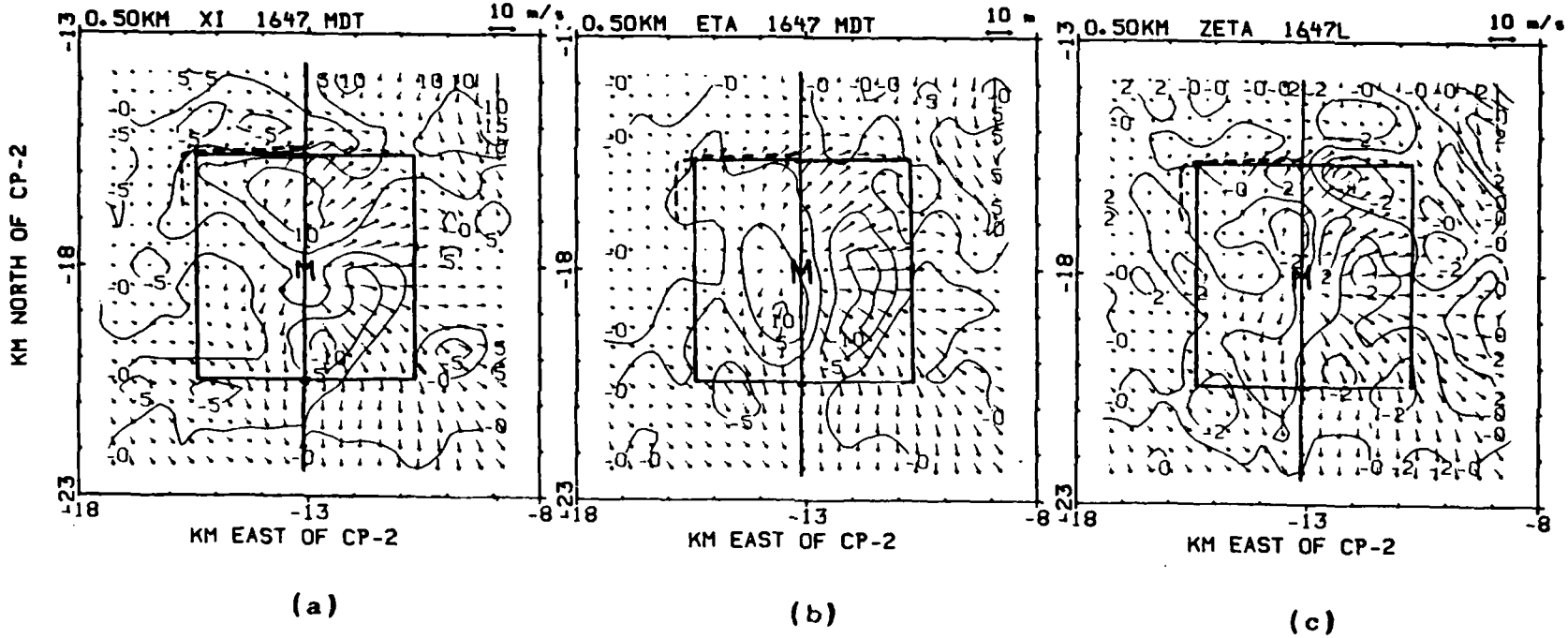

Figure 4.1: Plan view of horizontal velocity and contours of (a). ξ, (b). η, and (c). ζ for 14 July 1982, 1647 MDT at 0.5 km level. Microburst, M, microburst domain (small box), and south to north cross section (S-N) are also depicted.

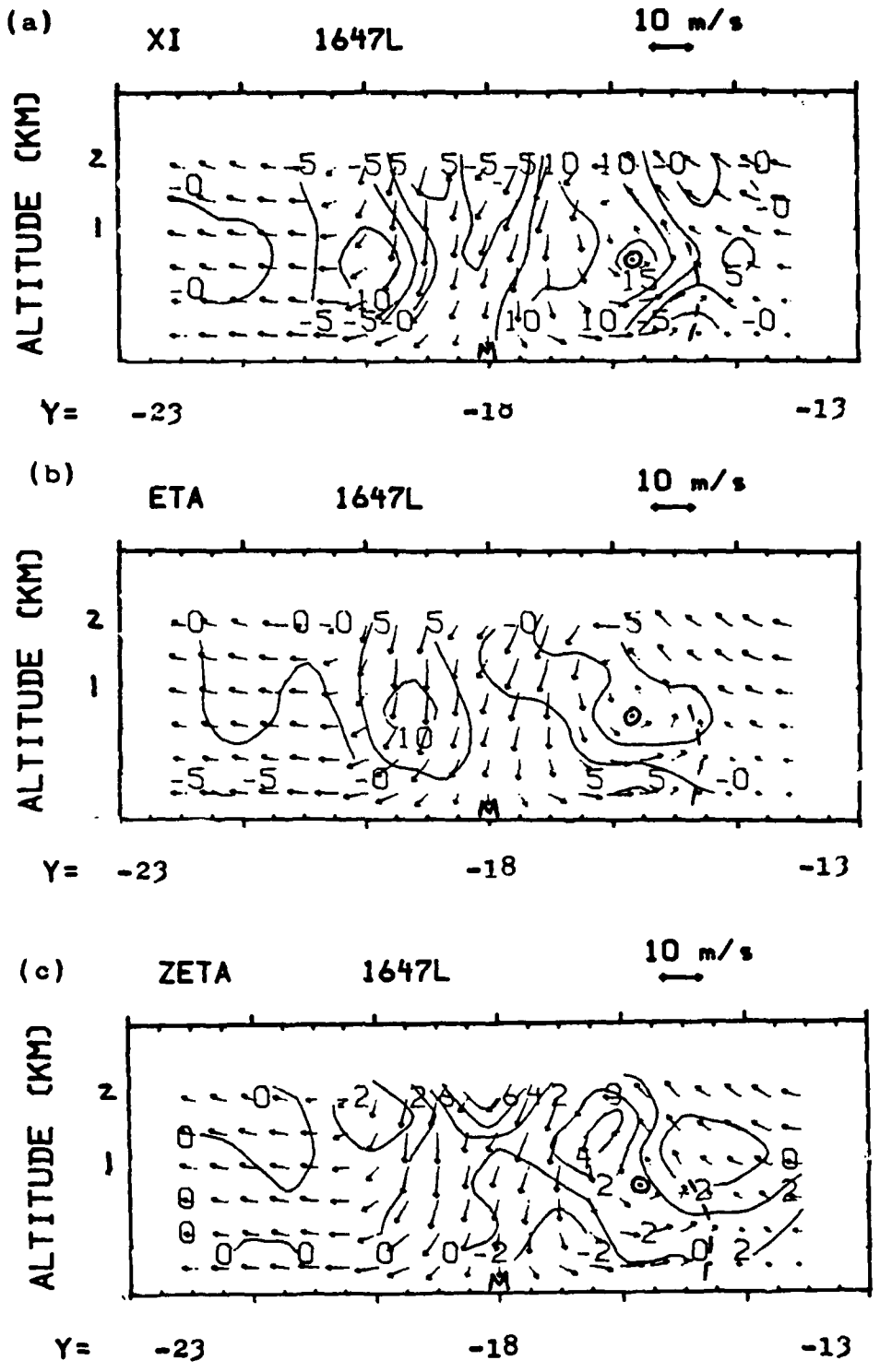

Figure 4.2: Vertical (S-N) cross section of (a) ξ, (b) η, and (c) ζ on wind field for 1647 MDT, 14 July 1982. Contoured values are times 10^{-3} s^{-1}. Gust front (dashed line) and rotor (⊙) are also depicted. North is to the right.

That is, the outflow to the north is going against the environmental flow while, to the south the outflow is in the same direction as the environmental flow; therefore, the rotor does not form. The ξ field is closed in the southern region, however, with a value greater than 10×10^{-3} per second, indicating a vortex of modest strength exists there.

Values of ξ are small at the microburst center up to at least 0.75 km, these are small compared to the relatively higher values along the periphery of the microburst. The flow in this region and in this plane may then be predominantly non-divergent or rotational, whereas on the south side of the microburst the flow perhaps is composed of a stronger divergent portion as well as a rotational portion. It follows then from this discussion that within the microburst center the flow is largely irrotational or divergent with respect to the y-z plane. The divergent idea follows straightforwardly while the irrotational aspect may not be as obvious. A cross-section of vertical velocity (Figure 4.3) shows the larger values of positive and negative ξ occur coincident with strong horizontal gradients of vertical velocity as we would expect.

Figure 4.1b shows the analyzed η field and Figure 4.2b shows this field in the S-N crossection. The maximum values (positive and negative) for η are found east and west of the microburst center. These maxima coincide with strong horizontal gradients of vertical velocity as did the ξ field

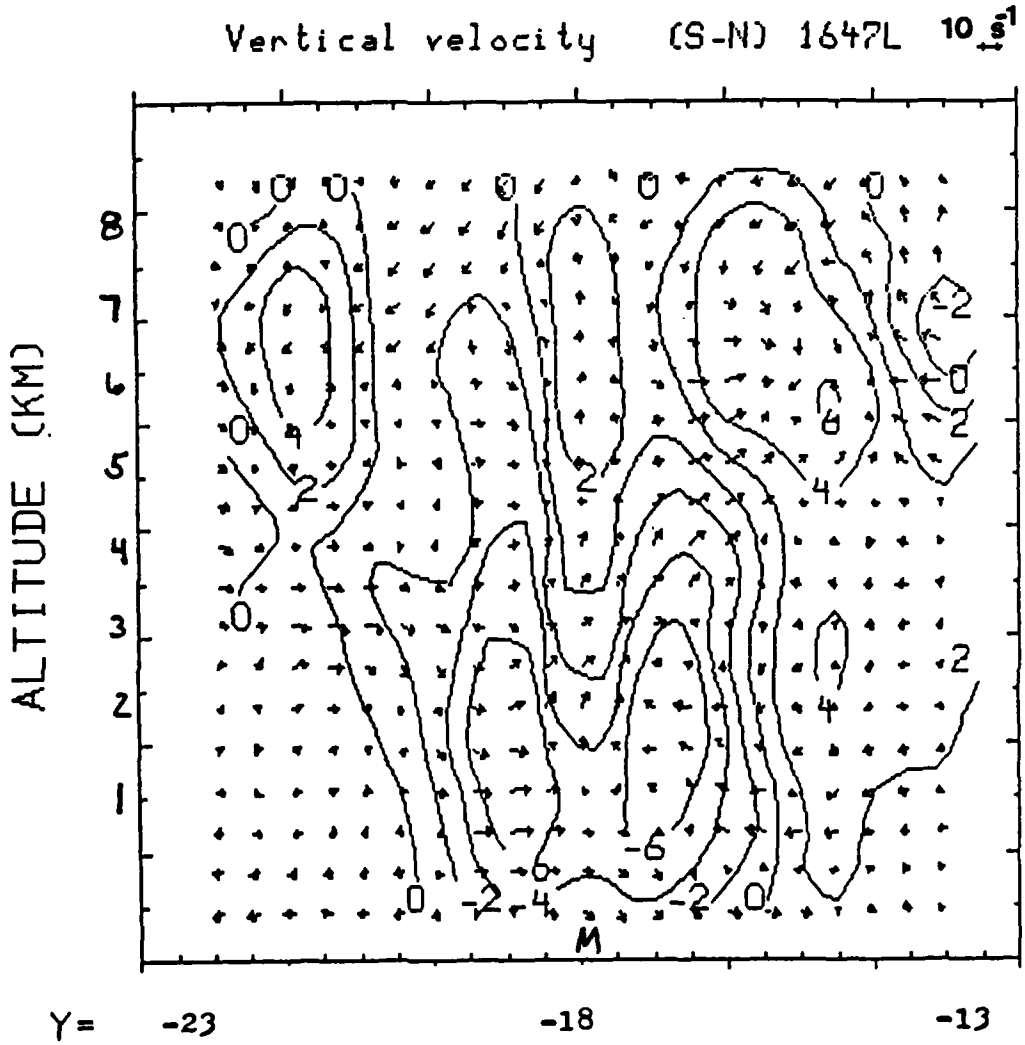

Figure 4.3: Vertical velocity (m/s) contoured on vector plot of in-plane vorticity field in S-N cross section for 1647 MDT, 14 July 1982.

(cross-section not shown). The actual centers are slightly weaker than the ξ values and are displaced in the downwind (south through southeast) direction indicating the impact of the environmental flow.

The ζ field is depicted in Figures 4.1c and 4.2c. Near zero values of ζ are found below 1 km at the microburst's center. This would signify that the flow is primarily divergent in this region, since we have already seen that ξ and η are also small here. ζ increases above 1 km to values greater than 5×10^{-3} per second. The microburst's irrotational structure below 1 km may act to spin down the positive ζ vorticity in this area. This 1 km level may be a transition area of rotation to divergence.

Also from Figures 4.1c and 4.2c, one develops an overall sense that this 3-dimensional vorticity field is largely a horizontal vector or at the very least quasi-horizontal in the periphery of the microburst. The values for ζ are generally one order of magnitude smaller than the horizontal components. Figure 4.4a depicts the horizontal vorticity components at 0.75 km combined to form a horizontal vector field. A vortex ring surrounds the microburst indicative of the strong shear in this region.

Fig. 4.4b illustrates the perturbation pressure field from Hughes (1987) for the 0.75 km level. It is plainly seen that the vortex ring lies in a region of low perturbation pressure which serves to accelerate the wind. Likewise, the rotor

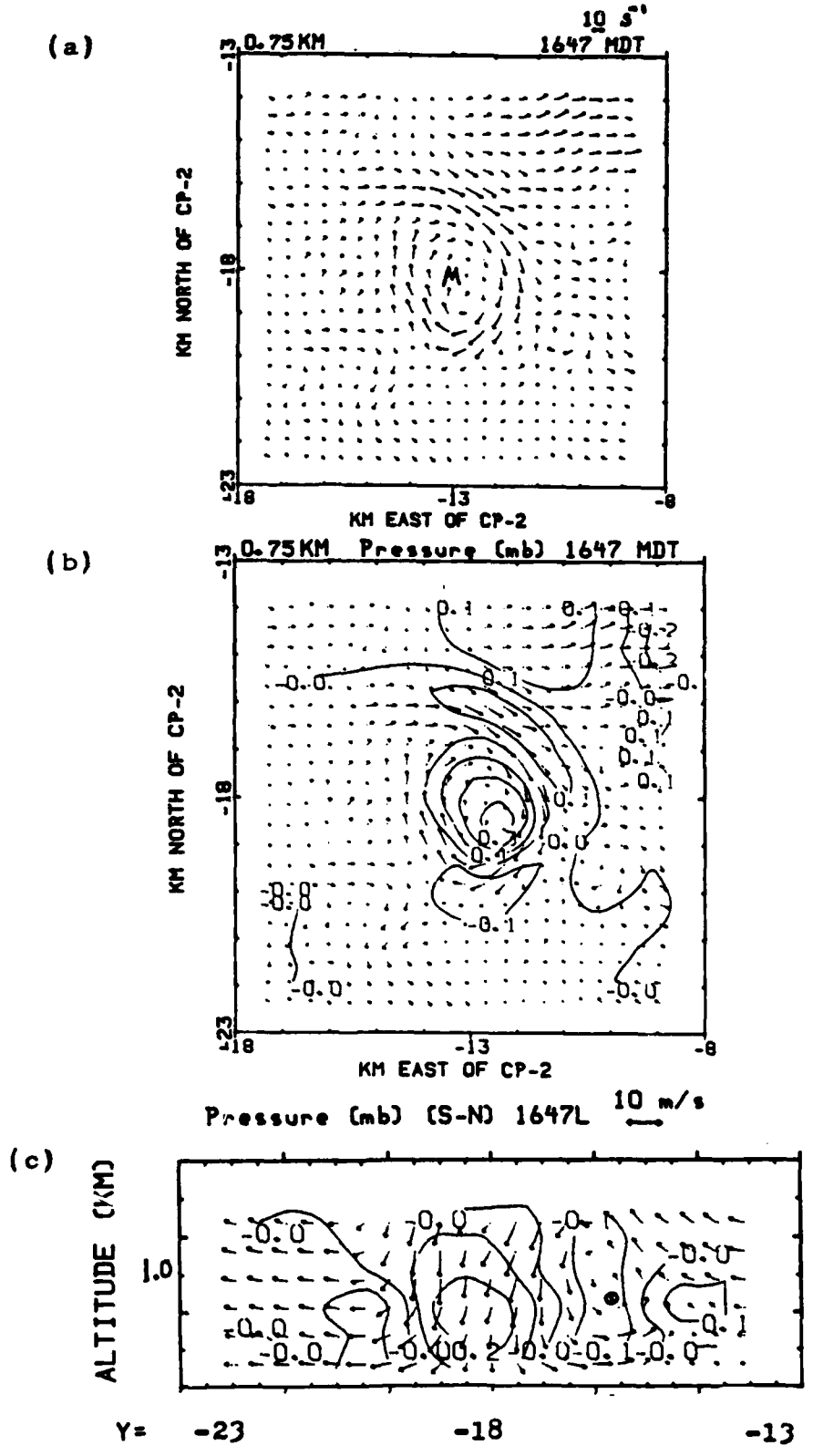

Figure 4.4: Plan view of (a) vorticity field at 0.75 km and (b) with the perturbation pressure field contoured. S-N cross section (c) of wind field with perturbation pressure field contoured for 1647 MDT, 14 July 1982.

itself is within the low perturbation pressure region as viewed in the S-N cross section in Fig. 4.4c. Parsons *et al.* (1987), Drogemeier and Wilhelmson (1987), and Kessinger *et al.* (1988) also suggest that these vortex circulations could be partly responsible for the observed high surface winds.

The vortices studied by Kessinger *et al.* (1988) moved away from the storm center. This has lead them to hypothesize about the possibility that variations in the strength of the downdraft may create separate centers of horizontal vorticity which then move down and away from the storm. The existence of horizontal vortices can be inferred from Fig. 4.2a and Fig. 4.2b on either side of the microburst. The vorticity centers are more evident in SW-NE cross section (not shown for 1647 MDT, see Fig. 4.7 for this cross section at 1649 MDT). Time resolution does not allow tracking of these vorticity centers, but some movement down and outward can be inferred between 1647 and 1649 MDT northeast of the microburst. This apparent movement could be a restablishment or a development of vorticity lower and further away as opposed to actual movement.

From the analyzed ζ field (Fig. 4.1c), this vortex ring oscillates through the plane at 0.75 km producing alternating regions of positive and negative ζ values. Finally, the strongest values of ζ are located above the 1 km level in the microburst area and at the eastern edge of the gust front while still being positive along the gust front, indicative of the existence of horizontal shear in these regions.

In order to determine typical magnitudes of the three vorticity components, area means and standard deviations were computed over the full storm domain and the microburst domain (box in Figure 4.1). These results are listed in Table 4.1. A comparison of root mean square values (standard deviations) in the table shows that the ξ and η components are the dominant components at every level. The ξ component is slightly larger than the η component in most cases. The rotor, which effects the vorticity field at levels 0.5 km through 1 km, and the predominant northerly flow to the northeast produce strong positive values of ξ (Figure 4.1a). This results in large positive values for the ξ areal means at these levels. The values for η and ζ are more varied, positively and negatively, and hence their areal means are smaller than that of ξ.

The same results hold for the microburst domain with the exception that the η component is strongest (rms value) at levels 0.75 and 1 km. Comparing across the domains, one finds the maximum positive and maximum negative values of each component over the grid illustrates the significance of the presence of the microburst, that is, these values occur in the microburst domain predominantly. Peak values of 1.9×10^{-2} and -1.6×10^{-2} per second for ξ and 1.7×10^{-2} and -1.7×10^{-2} per second for η at 0.75 km signifies the vortex ring resides mainly at this level as was shown by Figure 4.4a.

Table 4.1: Area mean (< >) and standard deviation (rms) values for each vorticity component over (a) storm domain and (b) microburst domain for 14 July 1982, 1647 MDT. Units are ($x10^{-4}$) s^{-1}.

(a)

Ht(km)	$\langle\xi\rangle$	ξ_{rms}	$\langle\eta\rangle$	η_{rms}	$\langle\zeta\rangle$	ζ_{rms}
0.25	-1.8	45.6	-3.5	29.0	0.87	15.6
0.50	13.5	46.5	-1.4	33.3	-0.22	14.9
0.75	28.5	50.5	-1.8	47.4	-1.9	14.4
1.00	19.8	40.7	-3.8	42.5	-1.9	17.1
1.50	3.5	41.4	-2.9	38.9	-0.06	19.9
2.00	-6.5	43.6	-0.4	38.1	1.4	22.9

(b)

Ht(km)	$\langle\xi\rangle$	ξ_{rms}	$\langle\eta\rangle$	η_{rms}	$\langle\zeta\rangle$	ζ_{rms}
0 25	9.9	46.7	-3.20	34.3	-0.60	15.9
0.50	18.4	50.5	-4.60	47.5	-3.50	14.6
0.75	24.6	68.6	-0.95	77.1	-2.70	13.2
1.00	21.2	55.7	3.60	64.0	-0.45	19.3
1.50	16.5	53.3	-0.48	53.1	1.20	24.0
2.00	10.7	53.8	-7.80	47.8	5.00	31.1

4.1.1 Budget Terms: Simple Case, 1647 MDT

Tables 4.2-4.7 list the results of the computed values of the terms in each of the component equations. They provide a level by level analysis of the areal mean and standard deviations for each of the four terms, horizontal advection (HAD), vertical advection (VAD), divergence (DIV), and tilting (TILT) for the storm domain (Tables 4.2-4.4) and the microburst domain (Tables 4.5-4.7). The arrows, $\langle\ \rangle$, indicate area means.

Since the area means for each component of the ξ, η, and ζ are at least one order of magnitude smaller than their standard deviations at each level, the standard deviations may be considered their typical values. Table 4.2 lists the budget terms for ξ, while budget terms for η and ζ are found in Table 4.3 and 4.4, respectively. HAD is the largest of all the terms for ξ and η budgets with VAD and TILT being the next higher terms, respectively. DIV is the smallest of all terms. TILT dominates the VAD term in the ζ budget and has the strongest typical value of all terms within the ζ budget at 0.75 km. It was shown earlier that the ξ component of vorticity was the strongest component and, therefore, its budget has the strongest terms of all three directions.

The last row in Tables 4.2-4.4 represent the vertical total of the area means for ξ with HAD, VAD, and TILT being nearly equal. HAD and TILT play opposite roles as source and sink for η (Table 4.3) as do VAD and DIV but to a lesser degree. It appears that the advection terms are nearly

Table 4.2: Area mean (< >) and standard deviation (σ) values for the terms of the x-component vorticity equation all for the storm domain for 14 July 1982, 1647 MDT. Units are ($x10^{-6}$) s^{-2}.

Ht(km)	<HAD>	HAD_σ	<VAD>	VAD_σ	<DIV>	DIV_σ	<TILT>	$TILT_\sigma$	<TEND>	$TEND_\sigma$
0.25	1.90	22.8	-2.2	11.2	0.25	4.1	0.33	8.2	0.99	26.9
0.50	0.93	21.4	-4.9	19.6	0.19	3.7	-0.04	9.2	0.65	26.9
0.75	-0.60	24.1	-1.0	15.1	-0.02	3.3	-0.07	8.1	2.3	27.7
1.00	0.02	24.1	4.4	17.0	0.09	3.4	0.84	6.4	3.9	27.4
1.50	-0.22	29.2	2.3	13.4	-0.15	3.5	0.08	7.4	1.1	29.5
2.00	-1.10	29.6	2.5	10.2	0.006	3.9	0.05	9.8	0.31	30.6
TOTAL	1.10		1.1		0.38		1.19		9.25	

Table 4.3: Area mean (< >) and standard deviation (σ) values for the terms of the y-component vorticity equation all for the storm domain for 14 July 1982, 1647 MDT. Units are ($x10^{-6}$) s^{-2}.

Ht(km)	<HAD>	HAD_σ	<VAD>	VAD_σ	<DIV>	DIV_σ	<TILT>	$TILT_\sigma$	<TEND>	$TEND_\sigma$
0.25	0.19	14.9	0.64	8.4	0.08	2.7	-0.54	7.9	0.48	20.8
0.50	0.38	20.7	1.40	15.6	0.09	2.1	-1.20	10.7	-0.22	30.1
0.75	1.7	25.2	0.79	13.7	-0.07	2.2	-1.30	11.2	-0.39	31.1
1.00	1.9	20.8	-1.30	13.4	-0.55	3.2	0.76	7.9	-0.24	24.2
1.50	0.006	20.0	-0.98	10.5	-0.34	3.6	0.36	6.8	-0.74	22.6
2.00	-1.1	22.2	0.22	12.1	0.28	3.2	-0.17	9.3	-0.22	26.0
TOTAL	3.08		0.77		-0.51		-2.09		-1.33	

Table 4.4: Area mean (< >) and standard deviation (σ) values for the terms of the z-component vorticity equation all for the storm domain for 14 July 1982, 1647 MDT. Units are ($x10^{-6}$) s^{-2}.

Ht(km)	<HAD>	HAD_σ	<VAD>	VAD_σ	<DIV>	DIV_σ	<TILT>	$TILT_\sigma$	<TEND>	$TEND_\sigma$
0.25	-0.51	7.6	0.26	5.4	-0.21	1.44	0.10	6.1	3.50	13.3
0.50	-0.40	9.4	0.73	5.8	-0.07	1.00	-0.61	6.9	2.20	12.6
0.75	-0.42	8.1	1.0	8.4	0.09	0.95	-0.86	9.8	1.98	14.4
1.00	-0.13	9.7	0.37	7.3	0.19	1.30	-0.79	8.0	1.60	13.9
1.50	-1.4	12.7	0.12	8.8	0.04	1.40	-0.22	8.2	-0.93	17.9
2.00	-1.7	13.3	1.2	7.7	0.05	0.80	-0.56	8.8	-2.20	18.1
TOTAL	-4.56		3.68		-0.09		-2.94		6.15	

Table 4.5: Area mean (< >) and standard deviation (σ) values for the terms of the x-component vorticity equation all for the microburst domain for 14 July 1982, 1647 MDT. Units are ($x10^{-6}$) s^{-2}.

Ht(km)	<HAD>	HAD_σ	<VAD>	VAD_σ	<DIV>	DIV_σ	<TILT>	$TILT_\sigma$	<TEND>	$TEND_\sigma$
0.25	3.80	35.9	-3.1	16.4	0.45	4.9	1.90	13.9	-8.4	45.6
0.50	-0.20	28.9	-6.6	28.2	-0.57	4.4	1.60	15.9	-9.1	38.8
0.75	-4.80	27.3	1.0	18.6	-0.25	3.3	1.40	11.0	-3.3	37.0
1.00	-1.40	20.3	8.3	24.5	1.30	3.7	2.90	8.7	4.5	37.4
1.50	0.48	25.5	3.6	19.1	0.84	4.6	0.49	10.7	4.0	32.1
2.00	-1.10	32.5	3.4	12.9	0.32	4.8	-0.42	15.2	4.5	37.7
TOTAL	-3.22		6.6		2.09		7.87		-7.8	

Table 4.6: Area mean (< >) and standard deviation (σ) values for the terms of the y-component vorticity equation all for the microburst domain for 14 July 1982, 1647 MDT. Units are ($x10^{-6}$) s^{-2}.

Ht(km)	<HAD>	HAD_σ	<VAD>	VAD_σ	<DIV>	DIV_σ	<TILT>	$TILT_\sigma$	<TEND>	$TEND_\sigma$
0.25	-0.55	23.6	2.4	13.2	0.36	3.8	-1.20	12.2	-7.60	37.0
0.50	0.64	33.6	5.7	24.2	-0.18	3.0	-0.17	17.4	-11.00	55.4
0.75	1.90	39.7	3.9	18.6	-0.09	3.2	-0.43	17.1	-6.10	54.4
1.00	2.90	26.6	-4.4	20.4	-1.60	3.7	0.32	10.7	-0.77	34.5
1.50	1.60	23.8	-2.6	14.2	-0.89	4.8	-0.007	9.2	1.99	26.6
2.00	-1.40	28.2	1.8	17.1	0.38	4.6	-0.72	13.1	6.60	35.3
TOTAL	5.09		6.8		-2.02		-2.21		-16.90	

Table 4.7: Area mean (< >) and standard deviation (σ) values for the terms of the z-component vorticity equation all for the microburst domain for 14 July 1982, 1647 MDT. Units are ($x10^{-6}$) s^{-2}.

Ht(km)	<HAD>	HAD_σ	<VAD>	VAD_σ	<DIV>	DIV_σ	<TILT>	$TILT_\sigma$	<TEND>	$TEND_\sigma$
0.25	0.43	11.6	0.37	8.7	0.03	1.3	0.63	9.2	-0.44	20.7
0.50	1.30	13.4	0.93	9.0	-0.22	1.2	-1.30	8.1	0.39	18.5
0.75	0.39	7.8	1.50	12.9	0.12	1.0	-2.50	13.0	-0.89	20.0
1.00	-0.14	10.7	3.50	9.9	0.18	1.4	-3.90	9.4	-0.02	17.0
1.50	-0.46	10.9	3.60	12.9	0.11	1.7	-3.50	9.8	1.20	21.5
2.00	-2.20	15.7	1.70	10.9	0.53	2.3	-0.66	11.7	2.50	23.9
TOTAL	-0.68		11.60		0.75		-11.20		2.74	

balanced by the divergence and tilting terms for this direction. The final budget, ζ, indicates that VAD is the source while the other terms are all acting to decrease positive ζ. This follows from the vertical cross section (Figure 4.2c) in that ζ was positive above 0.75 km for most of the storm domain.

Tables 4.5-4.7 lists the area mean and standard deviations for the microburst domain budget terms. As expected, the typical magnitudes (standard deviations) are larger in the microburst domain as compared to those in the storm domain for each term at virtually every level. The hierarchy of significance remains as in the storm domain as HAD, VAD, TILT, and DIV for the ξ and η budgets. The ζ budget again has VAD and TILT being very close in magnitude.

The vertically totalled area means are found in the last row of Table 4.5-4.7. In Table 4.5, HAD acts to decrease (sink) ξ, while the remaining terms provide a source of positive ξ. VAD and TILT have the largest totals, but the deficit attributed to HAD cuts the source due to VAD in half. The positive contributions from DIV and TILT are roughly five and six times, respectively, those at the storm domain. This points out the significance of the microburst flow field towards the generation of ξ.

The η budget in the microburst domain (Table 4.6) shows via the vertical total row the same trend as at the storm domain. That is, HAD and VAD are sources of η, while DIV and TILT are sinks. The largest change occurs with VAD and DIV

between domains. VAD develops to become the dominant source term and DIV increases fourfold to virtually match TILT as a sink. Yet again, the sources remain due to HAD and VAD.

VAD and TILT dominate the budget terms in the ζ component for the microburst domain. VAD is the source and TILT is the sink. The decrease in HAD seems to indicate the horizontal gradients of ζ are weaker on average than the vertical gradients. Furthermore, as VAD is acting to bring positive ζ values lower into the storm, TILT appears to single-handedly spin down the positive values. Figure 4.5 illustrates the opposing nature of these two terms in profile. The result of this interaction is to keep the ζ component of vorticity small and hence the 3-dimensional vorticity vector quasi-horizontal.

Although not evident from the vertical totals, HAD and VAD tend to oppose one another in vertical profile plots of their mean values. DIV and TILT then would be required to balance the result of the advection fields in order for vorticity to remain unchanged.

The last two columns in Tables 4.2 - 4.7 represent the areal mean and standard deviations for the respective tendency, i.e., $\partial\xi/\partial t$, etc. These were computed from the calculated values of the four terms of the vorticity component equations and not measured directly so care must taken in their interpretation. The tendency terms are less reliable than all the other terms in the vorticity budget equation. In addition to the uncertainities in u, v, and w estimates, the solenoidal

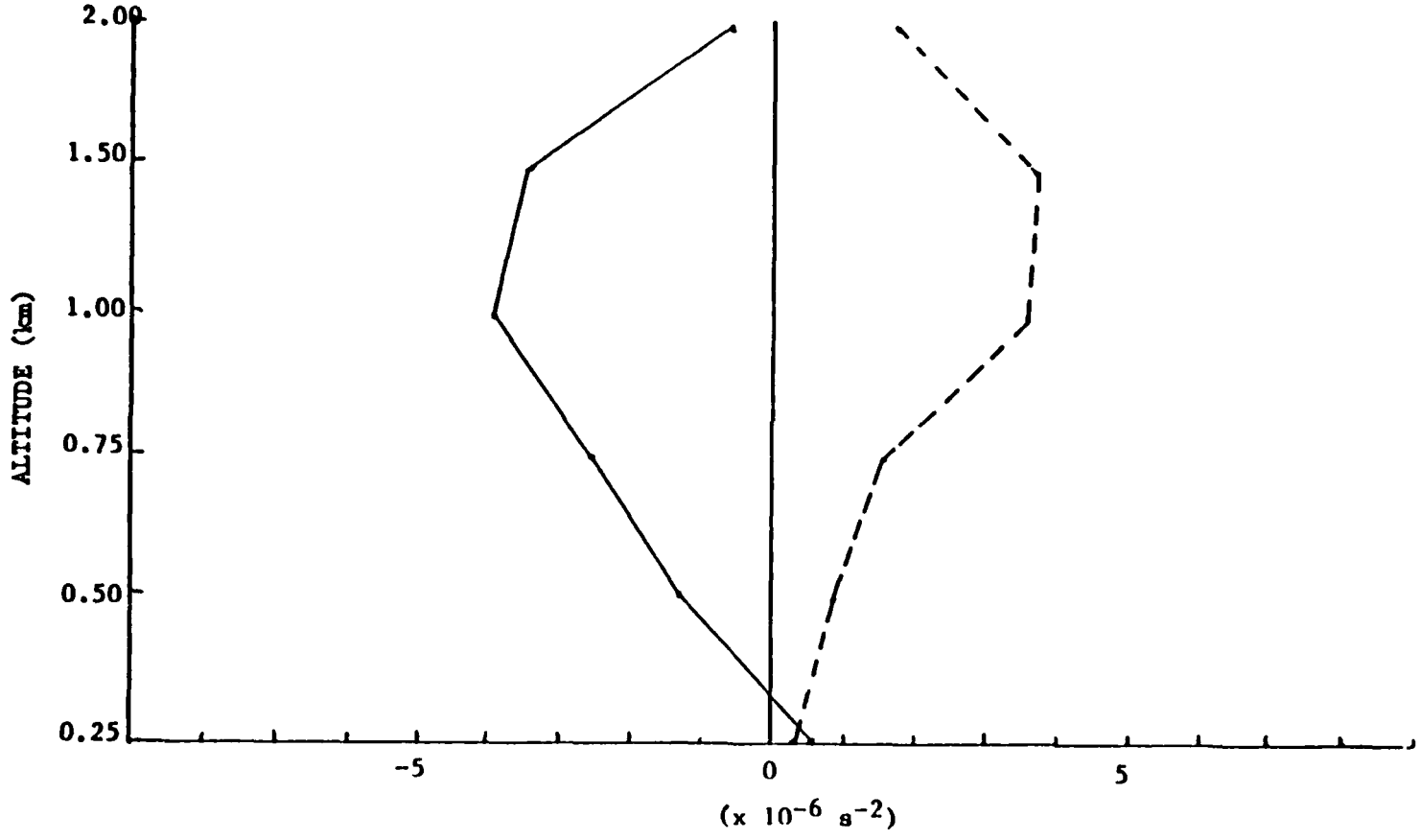

Fig. 4.5: Vertical profile of vertical advection (dashed line) and tilting term (solid line) for the ζ component equation over the microburst domain at 1647 MDT, 14 July 1982.

and frictional terms are excluded in the budget calculation. So these terms include the physical mechanisms affecting the respective vorticity component tendency, but also, errors in computing the three wind components and truncation errors. The truncation errors were minimized by using fourth-order finite difference schemes. Lin *et al.* (1987) found errors in the derived horizontal wind field to be about 1-2 meters per second. These errors are due to the statistical uncertainty of the radial velocity estimates and geometrical considerations. Estimates in vertical velocity lead to minimal errors when the anelastic continuity equation is integrated downward with a variational adjustment as was down in this storm (Lin *et al.*, 1987 and Lin and Coover, 1988). Further error analysis details are discussed by Hughes (1986), Lin *et al.* (1987), and Coover (1988). Errors due to the omission of the solenoidal and friction terms in budget calculations will show up in the tendency terms. That is, the budget terms not being balanced result in a larger (positive or negative) tendency term. Since the tendency term was not measured directly, no error can be made.

4.2 Simple Case: 14 July 1982, 1649 MDT

Figure 4.6a-4.6c depict the analyzed vorticity field overlain on the wind field for the 0.5 km level at 1649 MDT. Two new gust fronts have developed (dashed lines). ξ (Fig. 4.6a) has changed most noticeably along the gust fronts and the orientation of the field is now NW-SE, that is, parallel to the fronts. η has also increased (Fig. 4.6b) in magnitude

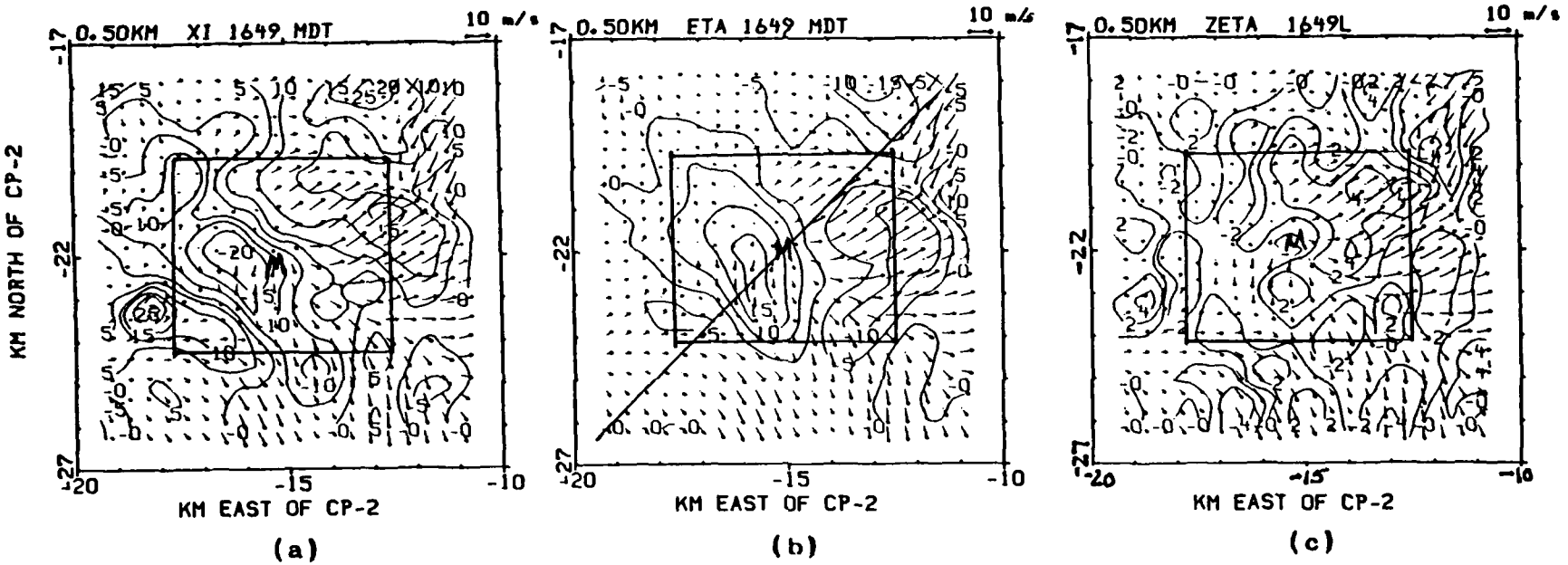

Figure 4.6: As in Fig. 4.1 except for 1649 MDT, 14 July 1982. SW-NE cross section is denoted (straight line).

mostly in the southwest region of the microburst domain. An increase in η is also apparent by a change in the coverage of the 10 x 10^{-3} s^{-1} isoline east of the microburst. Likewise, the ζ component (Fig. 4.6c) has become more positive along the gust front to the east of the microburst.

Figure 4.7a-4.7c is a SW-NE crossection through the center of the microburst with ξ (Fig. 4.7a), η (Fig. 4.7b), and ζ (Fig. 4.7c) overlain on the wind field. The ξ and η vorticity fields are essentially zero at the microburst center now through the full depth and ζ has become slightly positive. The storm is in its decay stage at this time as evidenced by the weaker vertical velocities in the microburst region. The gust front to the east appears to be better defined than the western gust front from a look at the winds in this cross section. In fact, the flow or horizontal gradient of the vertical velocity from the microburst center northeastward has produced a series of positive ξ vorticity centers with values in excess of 15 x 10^{-3} s^{-1}.

The western gust front is also evident in this cross section by the couplet of positive and negative ξ centers 1-3 km SW of the microburst center. Also of note here is the intensity of the horizontal wind outflow in these regions. The maximum outflow occurs below the maximum vorticity values. This was also shown by Kessinger *et al.* (1988) and Waranauskas (1985) to occur with their horizontal vortex circulations.

Figure 4.7: As in Fig. 4.2 except SW-NE cross section for 1649 MDT, 14 July 1982.

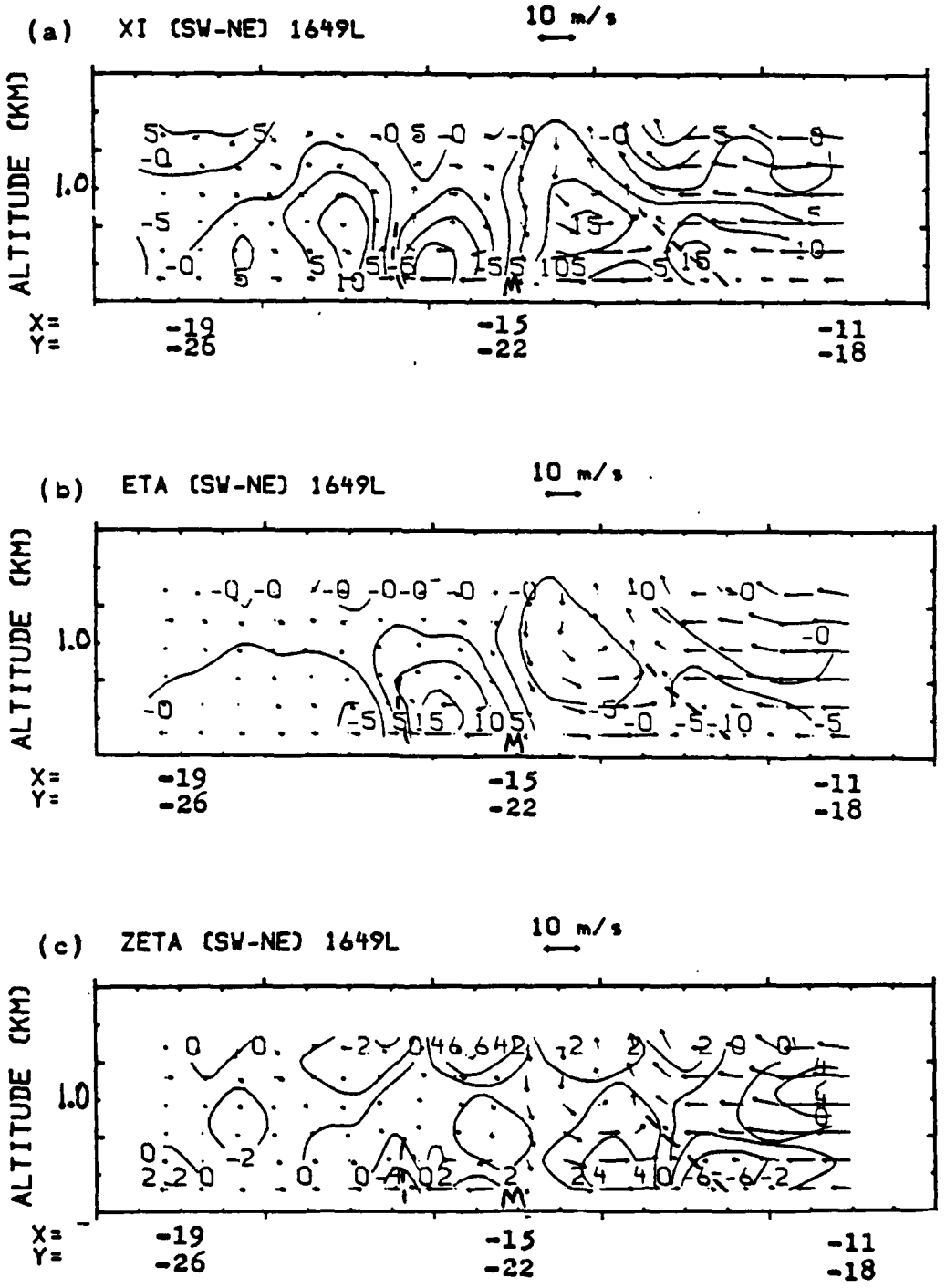

As in the 1647 MDT case, area means and standard deviations were computed (See Table 4.8). ξ is again the dominant vorticity component from a standard deviation or root mean square perspective in both the storm and microburst domains. The largest root mean square values for ξ and η now appear lower in the storm, 0.25 km - 0.75 km, than they were at 1647 MDT. This is also evident in Figure 4.7a and Figure 4.7b.

4.2.1 Budget Terms: Simple Case, 1649 MDT

The budget terms for the 1649 MDT time period are listed in terms of area means and standard deviations over the storm domain (Tables 4.9-4.11) and for the microburst domain (Tables 4.12-4.14). The first item of importance is the increased magnitude of the standard deviation for DIV in each direction over the 1647 MDT analysis time (See Figures 4.2 and 4.3 for comparison). These values have increased at least one order of magnitude for each component direction for levels below 1 km. The divergent flow destroys positive ζ and, at this time, the vertical shear has become significant in the lowest levels as the storm continues to decay. The result is that ξ and η are stronger in low level while ζ is strongest negative (positive) in low levels (higher levels) of the analysis volume.

The budgets of the three components at 1649 MDT are similar to those at 1647 MDT. The major change is the increased role that DIV and TILT play. It seems the vorticity associated with the 1647 MDT vortex ring establishes itself closer to the surface (See Table 4.8b). Figure 4.8 shows the ξ and η

Table 4.8: Area mean (< >) and standard deviation (rms) values for each vorticity component over (a) storm domain and (b) microburst domain for 14 July 1982, 1649 MDT. Units are ($x10^{-4}$) s^{-1}.

(a)	Ht(km)	$\langle\xi\rangle$	ξ_{rms}	$\langle\eta\rangle$	η_{rms}	$\langle\zeta\rangle$	ζ_{rms}
	0.25	15.10	78.5	-12.90	47.8	-2.80	28.7
	0.50	26.80	79.7	-16.40	54.8	-1.30	20.9
	0.75	35.50	70.0	-14.50	52.6	-0.26	20.3
	1.00	15.50	47.3	-17.90	36.1	-0.22	23.4
	1.50	0.62	42.1	0.94	28.7	1.10	23.7
	2.00	-5.60	47.6	0.18	29.1	2.40	22.5

(b)	Ht(km)	$\langle\xi\rangle$	ξ_{rms}	$\langle\eta\rangle$	η_{rms}	$\langle\zeta\rangle$	ζ_{rms}
	0.25	-10.20	92.1	12.2	64.4	6.8	30.8
	0.50	-0.41	88.5	12.6	70.0	2.4	20.2
	0.75	23.40	71.8	7.6	63.5	-1.2	19.2
	1.00	27.50	50.0	1.4	47.8	3.6	19.6
	1.50	14.20	37.2	-0.5	33.7	6.1	24.1
	2.00	15.70	41.0	-1.6	26.6	6.9	2.9

Table 4.9: Area mean (< >) and standard deviation (σ) values for the terms of the x-component vorticity equation all for the storm domain for 14 July 1982, 1649 MDT. Units are ($x10^{-6}$) s^{-2}.

Ht(km)	<HAD>	HAD_σ	<VAD>	VAD_σ	<DIV>	DIV_σ	<TILT>	$TILT_\sigma$	<TEND>	$TEND_\sigma$
0.25	3.10	44.9	-1.4	4.8	-1.60	26.1	1.60	21.3	1.7	66.2
0.50	-2.30	31.1	-3.8	11.9	2.20	17.1	-1.60	12.4	-5.6	39.1
0.75	-5.40	33.7	1.9	19.5	5.10	15.7	-1.30	9.3	0.4	38.9
1.00	-2.60	29.8	6.5	20.0	2.10	10.3	0.66	6.9	6.6	30.6
1.50	-0.59	33.4	3.8	15.5	-0.28	6.5	0.73	5.2	3.7	29.7
2.00	0.46	27.1	3.1	15.8	-1.10	6.7	0.30	6.4	2.8	28.8
TOTAL	-7.33		10.1		6.42		0.39		9.6	

Table 4.10: Area mean (< >) and standard deviation (σ) values for the terms of the y-component vorticity equation all for the storm domain for 14 July 1982, 1649 MDT. Units are ($x10^{-6}$) s^{-2}.

Ht(km)	<HAD>	HAD_σ	<VAD>	VAD_σ	<DIV>	DIV_σ	<TILT>	$TILT_\sigma$	<TEND>	$TEND_\sigma$
0.25	2.00	27.8	0.01	2.6	-0.93	19.1	-0.06	19.8	1.10	37.4
0.50	1.60	23.8	-0.59	8.0	-0.94	12.9	-4.10	15.0	-4.00	29.8
0.75	3.10	25.5	-2.00	13.7	-2.30	10.5	-3.50	14.2	-4.70	27.9
1.00	2.90	20.5	-1.80	9.3	-1.60	7.8	-0.14	10.3	-0.61	22.0
1.50	0.56	22.5	-1.10	7.1	-2.00	4.3	0.91	9.3	0.17	23.6
2.00	-0.93	19.7	-1.20	7.6	0.63	4.2	1.30	8.4	-0.23	22.4
TOTAL	9.13		-6.70		-7.14		-5.60		-8.27	

Table 4.11: Area mean (< >) and standard deviation (σ) values for the terms of the z-component vorticity equation all for the storm domain for 14 July 1982, 1649 MDT. Units are ($x10^{-6}$) s^{-2}.

Ht(km)	<HAD>	HAD_σ	<VAD>	VAD_σ	<DIV>	DIV_σ	<TILT>	$TILT_\sigma$	<TEND>	$TEND_\sigma$
0.25	2.10	22.1	-0.22	2.6	-1.10	9.9	-0.43	7.7	0.29	30.6
0.50	0.32	12.9	-0.89	5.5	-0.18	4.8	0.60	8.8	-0.14	20.4
0.75	-0.79	16.7	-0.80	6.6	0.74	3.8	1.00	10.5	0.16	20.2
1.00	-0.07	18.4	0.80	7.9	0.02	4.8	-0.32	7.9	0.43	23.1
1.50	-0.49	15.2	1.10	5.0	0.39	4.5	-0.61	6.7	0.41	20.0
2.00	0.88	11.8	1.40	9.6	-0.89	4.1	-1.30	9.2	0.19	19.2
TOTAL	1.95		1.39		-0.13		-1.06		1.34	

Table 4.12: Area mean (< >) and standard deviation (σ) values for the terms of the x-component vorticity equation all for the microburst domain for 14 July 1982, 1649 MDT. Units are ($x10^{-6}$) s^{-2}.

Ht(km)	<HAD>	HAD_σ	<VAD>	VAD_σ	<DIV>	DIV_σ	<TILT>	$TILT_\sigma$	<TEND>	$TEND_\sigma$
0.25	4.40	59.6	-1.9	4.1	-3.60	33.2	10.00	33.0	2.20	95.6
0.50	-10.60	32.1	-5.5	13.9	0.56	15.8	1.60	16.5	-4.30	47.8
0.75	-13.10	32.5	2.4	18.7	6.10	13.2	-0.47	10.4	-1.20	38.3
1.00	-3.10	24.6	7.7	15.5	4.20	11.8	2.20	8.1	2.80	31.4
1.50	-1.60	23.1	3.1	13.9	0.66	6.1	0.58	5.8	0.16	23.3
2.00	-0.13	25.1	1.7	12.5	-0.73	6.7	-0.43	6.5	-0.37	26.1
TOTAL	-24.13		7.5		7.20		13.48		0.31	

Table 4.13: Area mean (< >) and standard deviation (σ) values for the terms of the y-component vorticity equation all for the microburst domain for 14 July 1982, 1649 MDT. Units are ($x10^{-6}$) s^{-2}.

Ht(km)	<HAD>	HAD_σ	<VAD>	VAD_σ	<DIV>	DIV_σ	<TILT>	$TILT_\sigma$	<TEND>	$TEND_\sigma$
0.25	12.7	34.0	-0.28	3.1	-2.20	28.9	5.70	30.6	4.80	52.2
0.50	13.1	25.1	-1.80	11.1	-1.00	14.1	-1.20	21.1	3.00	31.3
0.75	12.9	19.3	-3.60	18.9	-3.80	11.0	-0.64	17.6	1.20	20.1
1.00	8.5	16.7	-2.20	9.6	-4.10	9.3	2.80	10.9	1.20	21.4
1.50	3.9	15.1	-1.20	8.6	-0.82	4.3	1.60	8.6	1.10	18.1
2.00	1.1	15.7	-1.40	9.4	-0.18	4.2	1.70	8.4	0.42	20.6
TOTAL	52.2		-10.48		-12.10		9.96		11.72	

Table 4.14: Area mean (< >) and standard deviation (σ) values for the terms of the z-component vorticity equation all for the microburst domain for 14 July 1982, 1649 MDT. Units are ($x10^{-6}$) s^{-2}.

Ht(km)	<HAD>	HAD_σ	<VAD>	VAD_σ	<DIV>	DIV_σ	<TILT>	$TILT_\sigma$	<TEND>	$TEND_\sigma$
0.25	3.3	26.8	-1.20	3.2	-4.40	13.0	-1.20	9.7	-0.76	36.8
0.50	-1.2	13.9	-2.40	6.2	-0.02	5.2	2.70	9.2	-0.12	21.4
0.75	-1.0	13.6	1.10	6.0	0.82	3.9	-0.42	0.5	0.31	20.9
1.00	1.5	13.4	3.80	7.8	0.09	4.4	-3.40	8.9	0.88	19.0
1.50	0.1	12.1	2.30	5.6	1.30	4.5	-2.30	5.5	0.56	17.8
2.00	2.9	12.5	0.77	8.9	-1.50	4.9	-1.90	7.7	0.27	16.8
TOTAL	5.6		4.37		-3.71		-6.55		1.14	

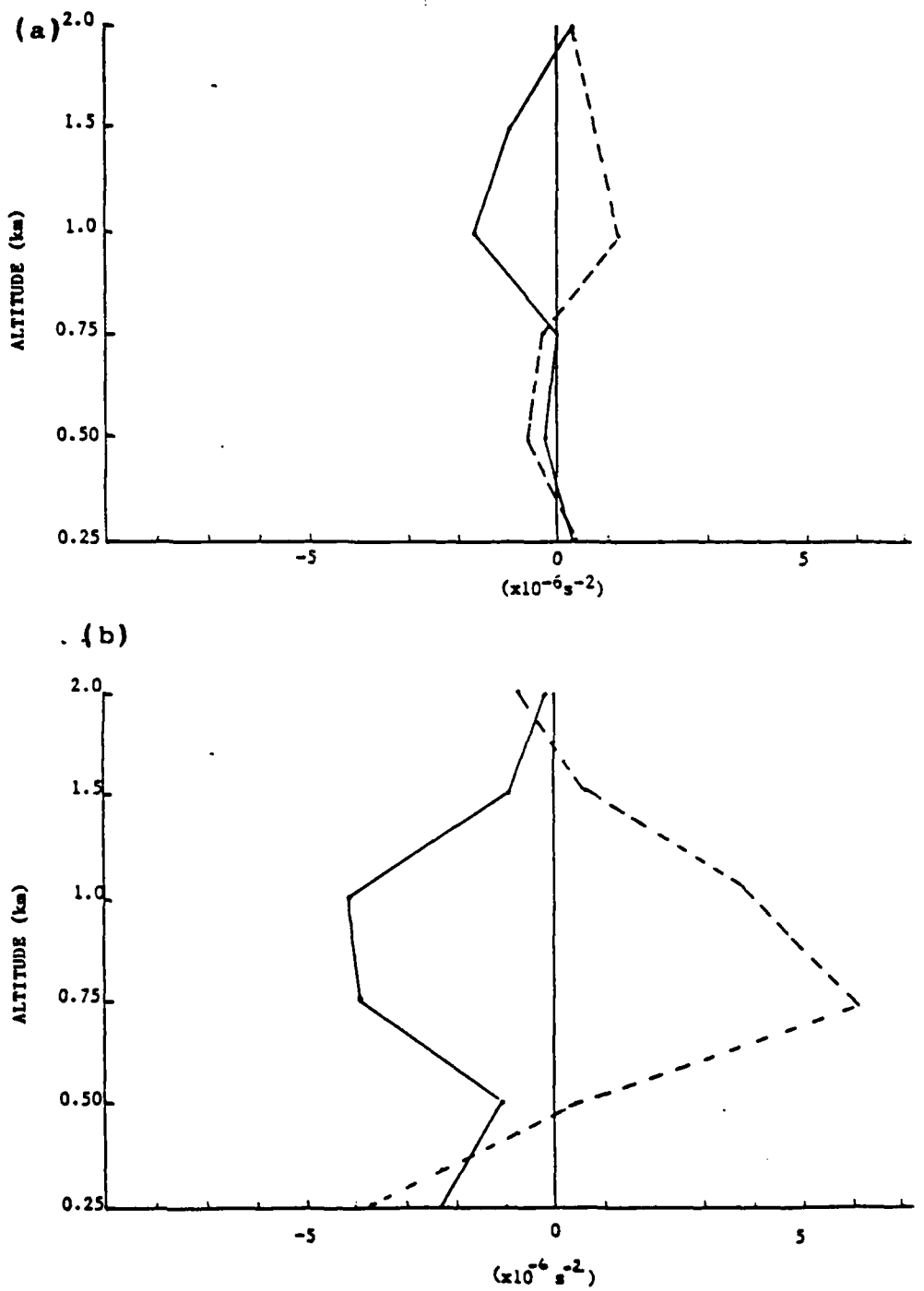

Fig. 4.8: Comparison of vertical profiles for x-direction (dashed line) and y-direction (solid line) vorticity divergence for (a) 1647 MDT and (b) 1649 MDT 14 July 1982.

divergence profiles for the microburst domain at both analysis times. The tilting profiles show a similar trend and, hence, are not shown here. The TILT and VAD terms are again compensating for the ζ budget so the vorticity remains quasi-horizontal.

4.3 Complex Case: 5 August 1982

The analyzed vorticity field for 1845 MDT at the 0.5 km level is presented on the wind field in Figure 4.9. This storm is more complicated than the previous case of 14 July 1982. As depicted in Fig. 4.9, this storm produced a microburst, M1 (-2,-24),a gust front, northeast through southeast (dashed line) of M1, and an enhanced downdraft, D (-6,-19). The complex interactions of the flow fields of the enhanced downdraft and M1 combine to create a large elongated region of the two horizontal components of vorticity from (-7,-17) to (-2,-21). This area corresponds to an area of low perturbation pressure gradient as retrieved by Coover (1988) (not shown), and is a feature found in horizontal vortex circulations (Kessinger *et al.*, 1988). A circulation is not found here, but rather, the horizontal vorticity is high. The actual shear then is not apparent simply by examining the Doppler derived wind field. The microburst domain (small box) encompasses M1, a large portion of the gust front, and the misocyclone, c_1. The inflowing environmental air is evident east of M1 at the bulge of the gust front.

4.3.1 X-direction Vorticity analysis (ξ)

ξ (Fig. 4.9) is overwhelmingly negative in the microburst domain at all levels with a pattern as shown here for the 0.5 km level. ξ is positive to the northwest as depicted in the

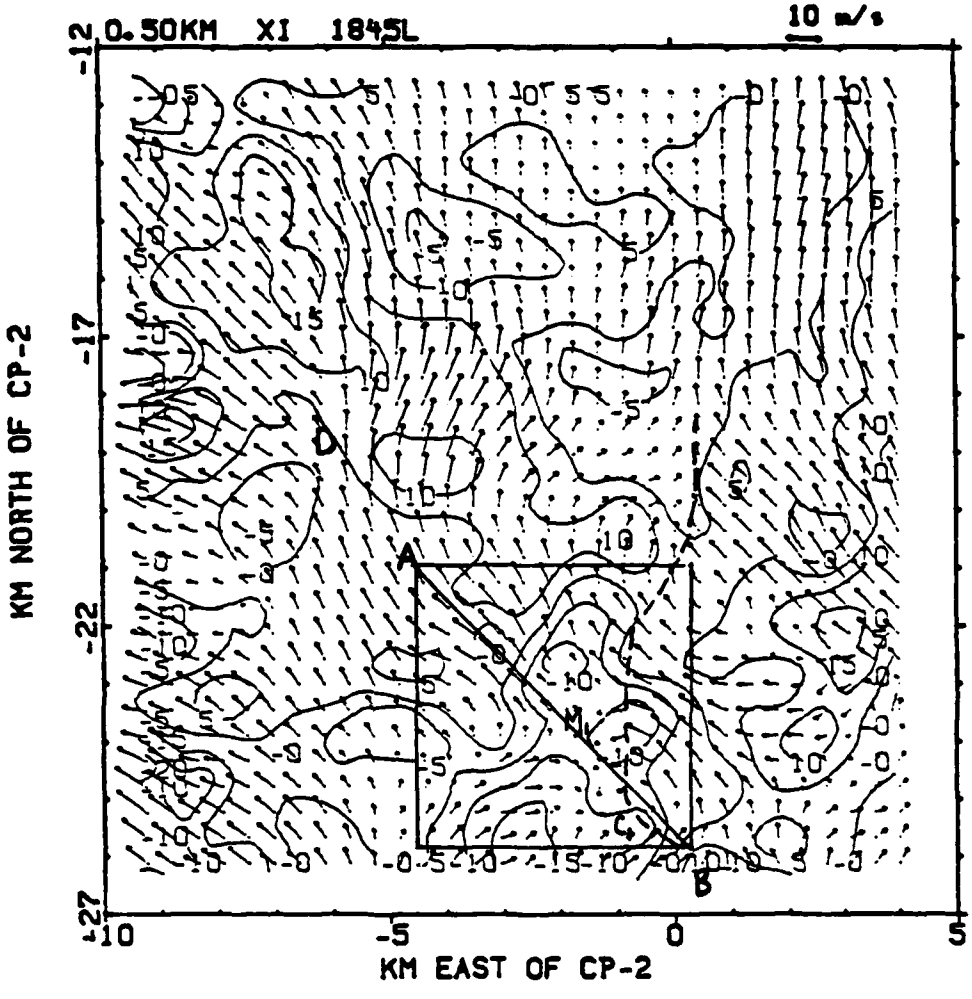

Figure 4.9: Plan view of horizontal velocity (arrows) field with ξ vorticity contoured (values are times 10^{-3} s^{-1}) for 1845 MDT, 5 Aug 82. Microburst domain (small box), gust front (dashed line), microburst M1, NW-SE cross section (A-B), mesocyclone-like vortex c1, and enhanced downdraft, D, are also depicted.

NW-SE crossection (A-B, Fig. 4.9) in Figure 4.10. Above 0.5 km, ξ is positive in this northwest quadrant. It is in this region that the divergent outflow of M1 is strongest in the lowest levels.

The reason for the distribution of ξ as largely negative south of M_1 and positive north can be seen from Fig. 4.10. The inflowing air velocity increases with height south of M_1, i.e., $\partial v/\partial z$ is positive and decreases strongly in the north. This results in the given 1845 MDT ξ distribution. By 1850 MDT, the only real change is the most shallow layer of maximum outflow winds to the north, i.e., $\partial v/\partial z$ is large negative and therefore, ξ is large positive ($\partial w/\partial y$ is weak).

ξ values change very little between 1845 and 1847 MDT (Fig. 4.11). From Tables 4.15 and 4.16 only a slight increase in the mean values of ξ in low levels below 1 km over both domains and a decrease above 1 km is detected. Root mean square values remain the same.

By 1850 MDT, ξ continues virtually unchanged at 0.5 km (Fig. 4.12) except for the northwest quadrant of the microburst domain. Over the storm domain, the elongated region of strong ξ values mentioned at 1845 MDT from north of D, to north of M1 has intensified. The perturbation pressure field has also lowered in the same regions (Fig. 4.13). A band of strong positive ξ values 10×10^{-3} s^{-1} to 20×10^{-3} s^{-1} to 15×10^{-3} s^{-1} lies west southwest to north of M1. The wind field in this region curves anticyclonically (at 0.5 km) emanating from the

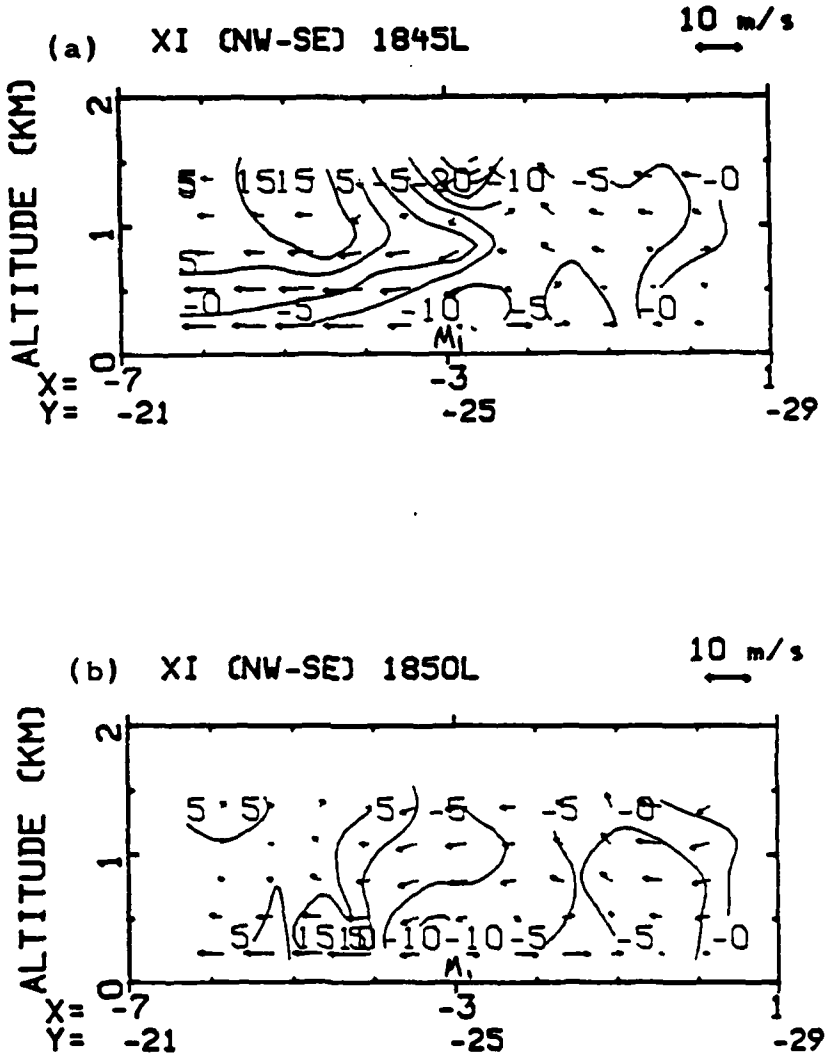

Fig. 4.10: NW-SE vertical cross section of ξ vorticity contoured on wind field for (a) 1845 MDT and (b) 1850 MDT, 5 August 1982. Location of microburst, M1 is indicated.

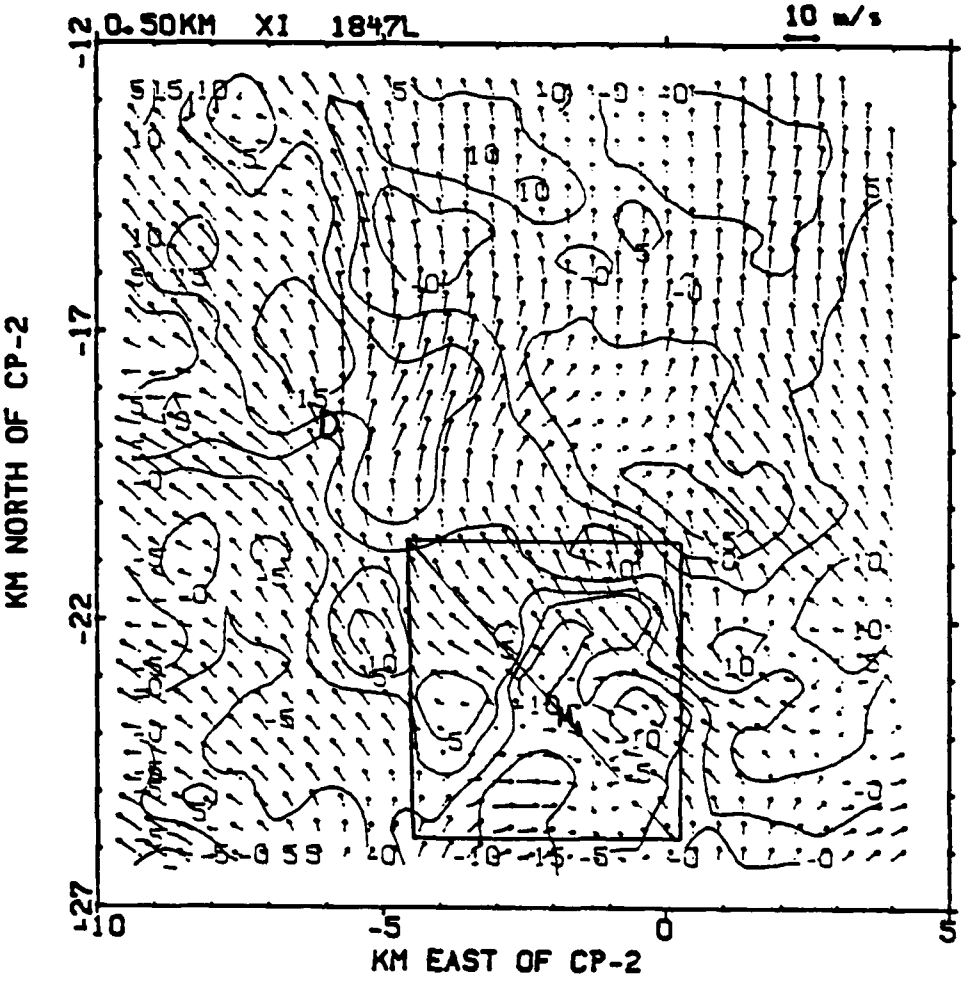

Fig. 4.11: Same as Fig. 4.9 except for 1847 MDT, 5 August 1982.

Table 4.15: Area mean (< >) and standard deviation (σ) values for each vorticity component over the storm domain for (a) 1845, (b) 1847, and (c) 1850 MDT, 5 Aug 1982. Units are ($x10^{-3}$) s^{-1}.

(a)

Ht(km)	$\langle\xi\rangle$	ξ_{rms}	$\langle\eta\rangle$	η_{rms}	$\langle\zeta\rangle$	ζ_{rms}
0.25	0.69	6.3	-2.40	6.6	0.12	2.9
0.50	1.8	6.3	-1.60	6.3	0.20	3.0
0.75	3.4	6.2	-0.51	5.9	0.28	3.1
1.00	3.8	4.8	-0.02	4.9	0.29	3.2
1.25	3.7	5.5	0.11	5.1	0.24	3.2

(b)

Ht(km)	$\langle\xi\rangle$	ξ_{rms}	$\langle\eta\rangle$	η_{rms}	$\langle\zeta\rangle$	ζ_{rms}
0.25	1.7	6.3	-1.5	6.8	0.15	3.1
0.50	2.6	6.2	-1.3	6.4	0.19	3.2
0.75	3.8	6.2	-0.95	5.9	0.26	3.3
1.00	3.4	5.2	-0.95	3.6	0.32	3.4
1.25	2.7	6.0	-1.1	2.4	0.19	3.7

(c)

Ht(km)	$\langle\xi\rangle$	ξ_{rms}	$\langle\eta\rangle$	η_{rms}	$\langle\zeta\rangle$	ζ_{rms}
0.25	2.2	7.4	-1.5	7.0	0.19	3.0
0.50	3.0	6.6	-1.6	6.2	0.21	3.2
0.75	4.2	6.2	-1.4	5.4	0.31	3.4
1.00	4.5	5.5	-0.65	4.7	0.38	3.4
1.25	4.4	5.6	-0.07	4.8	0.30	3.6

Table 4.16: Same as Table 4.15 except for the microburst domain.

(a)

Ht(km)	$\langle\xi\rangle$	ξ_{rms}	$\langle\eta\rangle$	η_{rms}	$\langle\zeta\rangle$	ζ_{rms}
0.25	-6.50	6.5	-2.50	11.6	0.46	4.7
0.50	-4.30	6.4	-1.10	10.0	0.98	4.4
0.75	-1.00	7.3	0.47	5.8	1.2	3.9
1.00	0.78	6.5	0.74	5.1	1.2	4.2
1.25	1.40	8.7	0.88	5.8	1.0	4.2

(b)

Ht(km)	$\langle\xi\rangle$	ξ_{rms}	$\langle\eta\rangle$	η_{rms}	$\langle\zeta\rangle$	ζ_{rms}
0.25	-4.50	6.1	-3.3	9.4	0.49	4.9
0.50	-3.80	6.1	-3.2	9.4	1.17	4.8
0.75	-1.60	7.7	-1.7	8.4	1.34	4.6
1.00	0.08	7.7	1.3	4.6	1.26	4.4
1.25	0.43	8.9	-1.0	2.9	1.59	4.7

(c)

Ht(km)	$\langle\xi\rangle$	ξ_{rms}	$\langle\eta\rangle$	η_{rms}	$\langle\zeta\rangle$	ζ_{rms}
0.25	-1.87	9.2	-3.62	9.6	0.48	4.1
0.50	-0.82	8.1	-2.47	8.7	0.99	4.4
0.75	0.70	8.2	-0.02	6.9	1.22	4.6
1.00	2.22	7.3	2.15	5.0	1.40	4.0
1.25	3.19	7.6	3.06	5.0	1.48	3.8

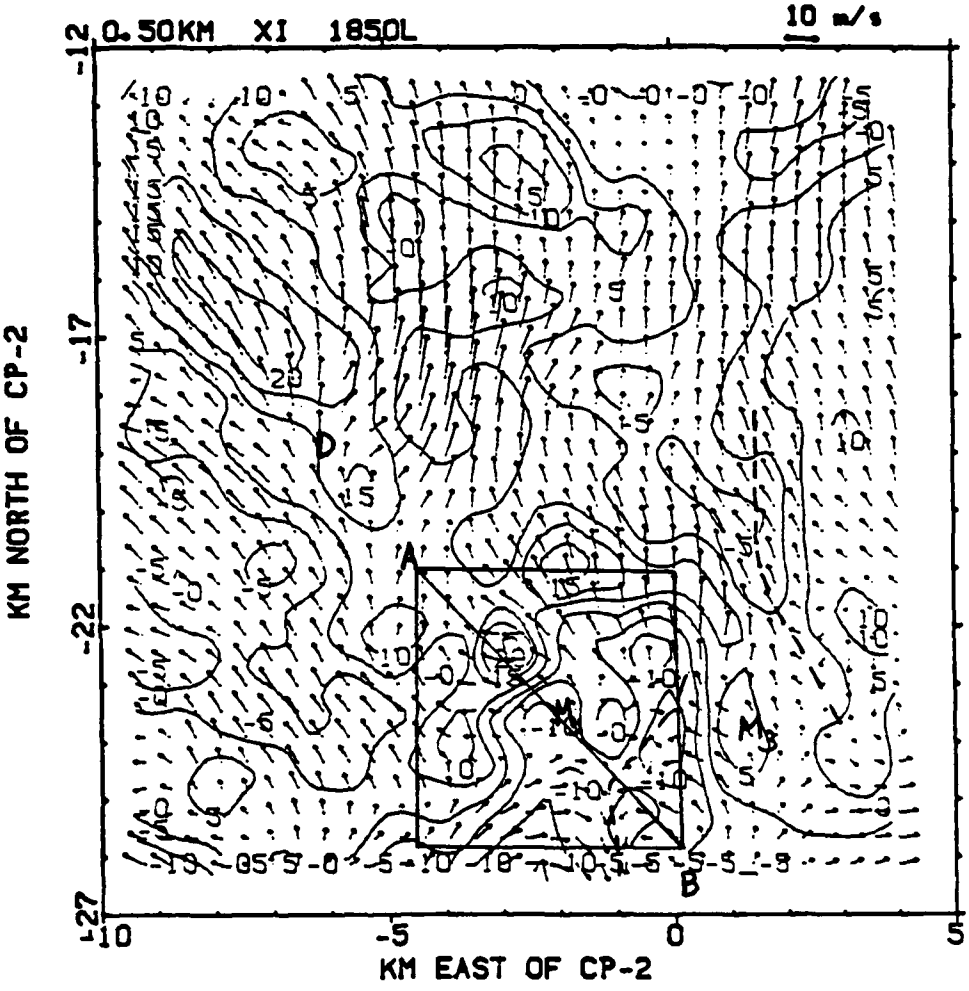

Fig. 4.12: Same as Fig. 4.9 except for 1850 MDT, 5 August 1982.

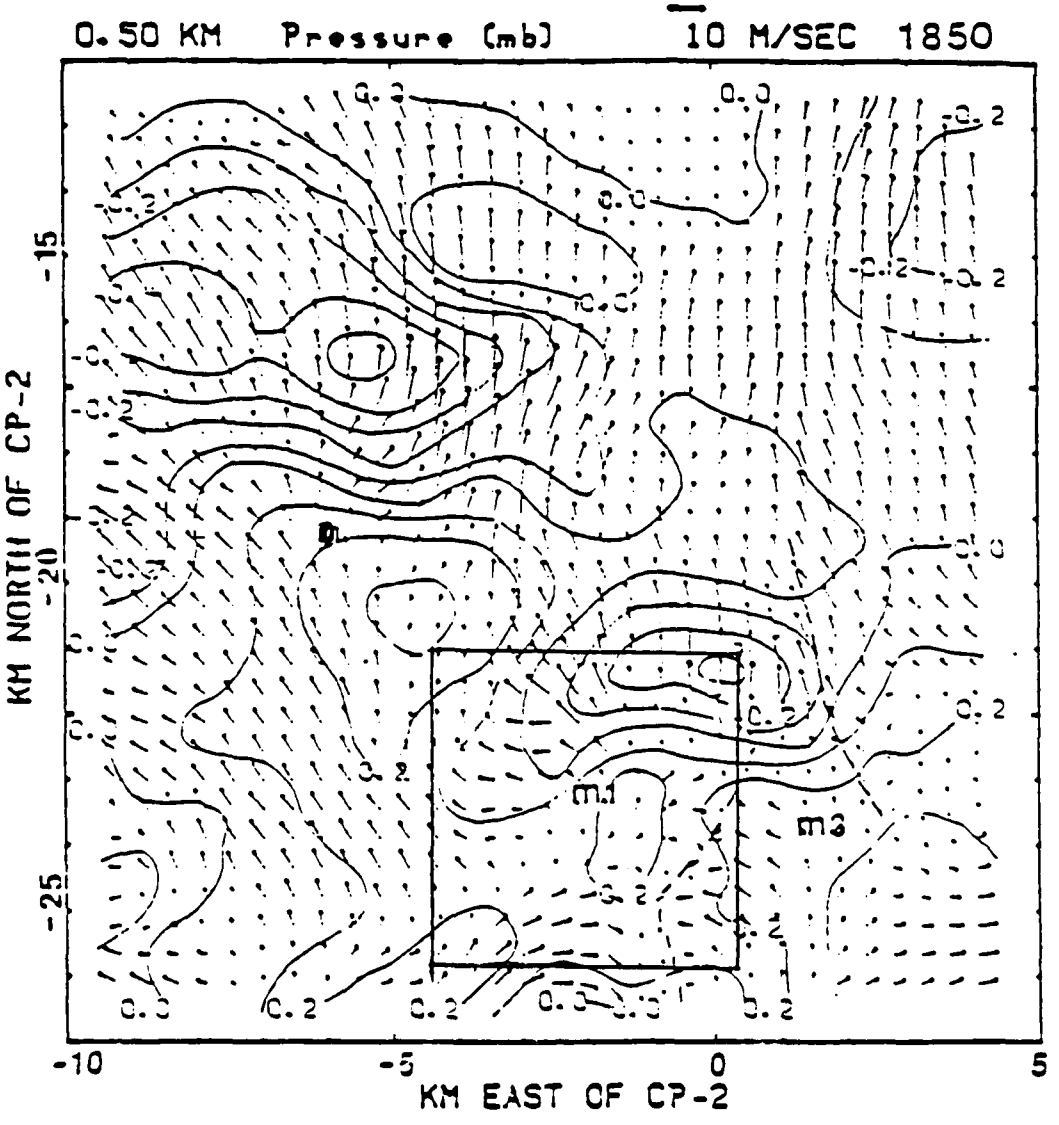

Fig. 4.13: Plan view of the perturbation pressure field, for the 5 August 1982, 1850 MDT case at 0.50 km, for 0.5 km grid spacing (From Coover, 1988).

high perturbation pressure dome (0.2 mb) associated with M1 into a lower pressure region between both M1 and the high pressure dome associated with D.

Table 4.15c and 4.16c also shows that at 1850 MDT, ξ increases in the area mean at all levels in the storm domain and microburst domain. In fact, the largely negative ξ mean values in low levels that existed at 1845 and 1847 MDT have all but been reversed in the mean by 1850 MDT. This indicates the strengthening of a positive ξ field as shown in Figure 4.12 northwest of M1. Figure 4.10 illustrates the stronger vertical shear at 1850 MDT responsible for the stronger positive ξ values.

4.3.2 ξ Budget Terms

Figure 4.14 illustrates the change in $\langle\xi\rangle$ (where $\langle\ \rangle$ represents area mean) through each time period in vertical profile for the microburst domain. It can be seen that ξ is increased each time below 0.5 km and consistently increases with height at each time period. Above 0.5 km, $\langle\xi\rangle$ at 1845 MDT decreases slightly by 1847 MDT, but is again increased at 1850 MDT.

Table 4.17 lists the area mean and standard deviation values for each of the four budget terms. At 1845 MDT (Table 4.17a) in the storm domain, a balance must be accomplished between HAD and the combined effect of DIV and TILT since VAD is small. A balance is not met and by comparing vertical

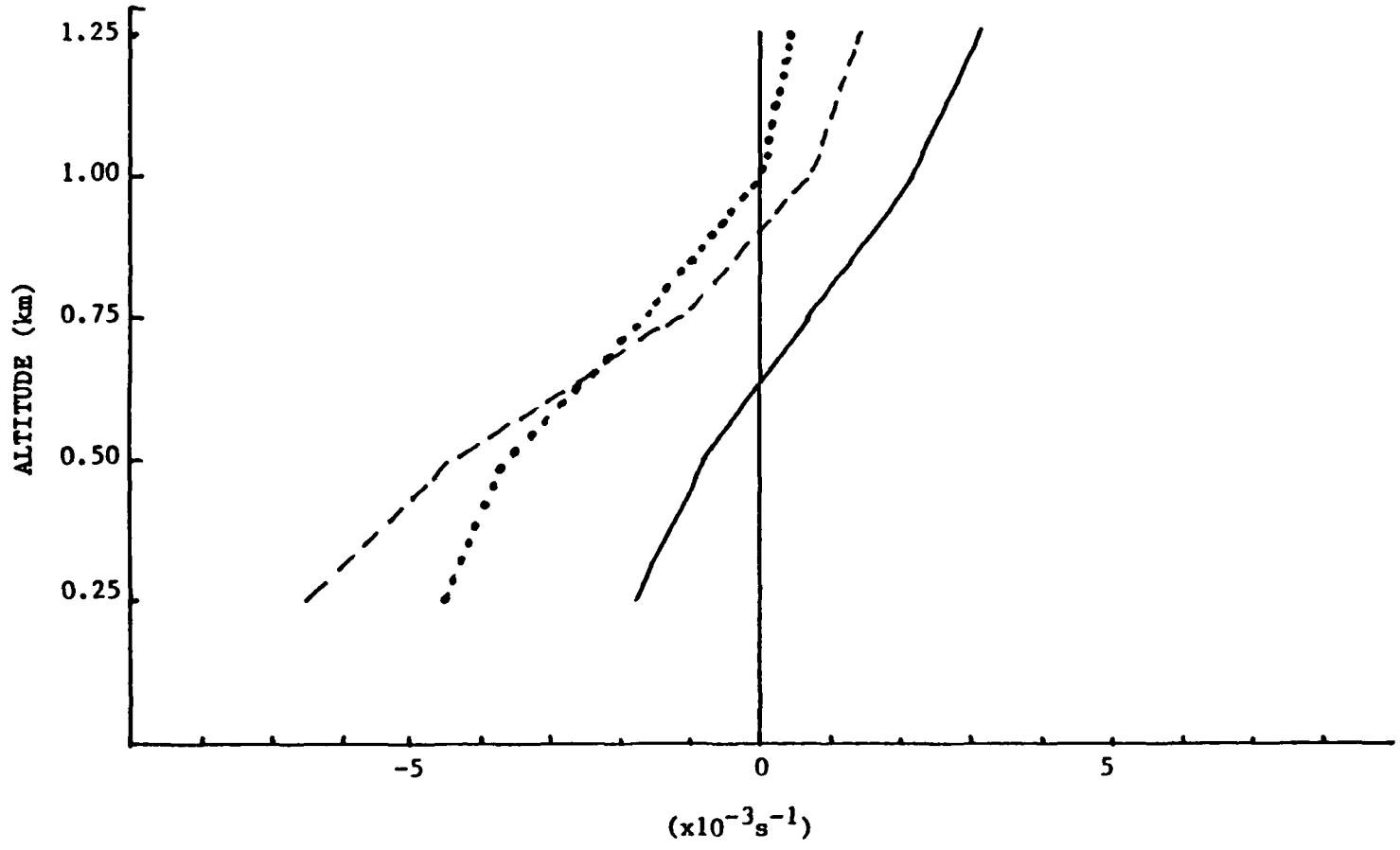

Fig. 4.14: Vertical profile of area mean values of ξ vorticity at 1845 (dashed line), 1847 (dotted line), and 1850 MDT (solid line) 5 August 1982.

Table 4.17: Area mean (< >) and standard deviation (σ) values for the terms of the x-component vorticity equation over the storm domain for (a) 1845, (b) 1847, and (c) 1850 MDT, 5 Aug 1982. Units are ($x10^{-6}$) s^{-2}.

(a)

Ht(km)	<HAD>	HAD_σ	<VAD>	VAD_σ	<DIV>	DIV_σ	<TILT>	$TILT_\sigma$
0.25	4.20	39.5	0.009	2.7	-1.30	16.9	1.20	19.0
0.50	3.30	34.8	0.33	8.7	-1.30	9.9	1.70	17.3
0.75	0.92	30.6	0.59	10.0	-0.63	9.5	-0.52	16.8
1.00	-0.61	30.1	0.03	13.0	0.49	10.1	-1.20	16.2
1.25	-3.50	44.3	-0.42	15.9	0.72	13.7	-1.70	20.9
TOTAL	4.31		0.54		-2.02		-0.52	

(b)

Ht(km)	<HAD>	HAD_σ	<VAD>	VAD_σ	<DIV>	DIV_σ	<TILT>	$TILT_\sigma$
0.25	4.3	45.1	0.15	2.6	-1.70	14.6	2.3	20.3
0.50	2.8	36.8	0.53	8.9	-1.30	12.1	2.2	17.5
0.75	0.6	33.8	0.63	11.0	-0.94	11.4	1.2	17.1
1.00	1.2	29.9	0.46	15.5	0.21	10.2	0.15	10.5
1.25	1.6	35.5	0.51	19.4	-0.94	11.3	0.94	18.9
TOTAL	10.5		2.28		-4.67		6.79	

(c)

Ht(km)	<HAD>	HAD_σ	<VAD>	VAD_σ	<DIV>	DIV_σ	<TILT>	$TILT_\sigma$
0.25	5.0	55.0	0.04	2.8	-2.40	20.8	4.65	24.4
0.50	2.3	39.2	-0.11	9.5	-1.20	12.0	2.98	21.7
0.75	-1.2	31.8	-0.06	12.2	0.27	9.4	-0.65	20.5
1.00	-1.6	26.1	1.04	12.6	1.40	12.0	-0.95	18.3
1.25	-2.7	29.9	1.62	13.4	1.63	10.2	-1.60	20.3
TOTAL	1.8		2.53		-0.30		3.83	

totals, a net increase of ξ is suggested. By 1847 MDT (Table 4.17b), the contribution from VAD has increased slightly (level by level) but is still one order smaller in the mean than the remaining terms. At this time, HAD and TILT acting positively (source) at low levels overwhelms the loss through DIV. Across each time period, it is apparent that the DIV term is the sole generator of negative ξ. The remaining terms generate positive ξ with the strongest generation occuring below 0.75 km.

In the smaller microburst domain (Table 4.18), the area mean and root mean square (standard deviation) values are larger than at the storm domain. From Fig 4.9 it is evident that due to the overwhelming negative ξ field, HAD would act as a sink as the table indicates. VAD counters by acting as a source. TILT is a source at each time period with maximum contribution ocurring at 1847 MDT. The large horizontal gradients of ξ create a very strong HAD term leading to removal of positive ξ within the microburst domain over time. VAD and TILT counteract this removal mechanism and dominate at 1845 MDT and 1847 MDT. By 1850 MDT when the ξ gradient is strongest, DIV acts with VAD and TILT to attempt a balance. As the ξ field gets stronger, the DIV term especially to the north of M_1 becomes a strong source.

4.3.3 Y-direction Vorticity Analysis (η)

Between 1845 and 1850 MDT, $\langle\eta\rangle$ values remain predominantly negative (Table 4.15 and 4.16) over the storm domain and below 1 km in the microburst domain. A tight gradient of η

Table 4.18: Same as Table 4.17 except for microburst domain.

(a)

Ht(km)	<HAD>	HAD_σ	<VAD>	VAD_σ	<DIV>	DIV_σ	<TILT>	$TILT_\sigma$
0.25	-9.40	45.8	1.00	5.3	4.5	33.4	-5.90	34.6
0.50	-4.80	36.9	3.70	16.9	-3.8	15.5	7.30	28.7
0.75	-4.70	46.1	1.90	17.3	-1.4	11.8	0.16	18.9
1.00	0.46	37.5	-0.16	24.2	-2.0	17.1	3.20	25.5
1.25	2.00	53.4	0.68	31.8	-1.7	19.5	6.20	29.6
TOTAL	-16.40		7.12		-4.4		10.96	

(b)

Ht(km)	<HAD>	HAD_σ	<VAD>	VAD_σ	<DIV>	DIV_σ	<TILT>	$TILT_\sigma$
0.25	-6.40	66.7	0.46	5.1	-0.39	26.1	-1.70	32.7
0.50	-11.00	58.8	2.49	15.9	-1.79	18.5	0.43	26.5
0.75	-11.60	56.9	6.02	16.3	-2.16	15.7	3.22	22.4
1.00	-4.00	56.1	4.94	20.0	-1.14	17.6	5.61	27.7
1.25	0.96	67.4	2.35	25.2	-3.39	24.4	8.85	38.2
TOTAL	-32.04		16.26		-8.87		16.41	

(c)

Ht(km)	<HAD>	HAD_σ	<VAD>	VAD_σ	<DIV>	DIV_σ	<TILT>	$TILT_\sigma$
0.25	-16.1	100.9	2.4	5.6	2.8	42.0	0.25	41.2
0.50	-20.9	66.5	7.7	18.7	1.3	18.7	4.55	34.5
0.75	-19.0	49.7	7.7	22.2	2.3	13.6	3.51	31.9
1.00	-10.1	36.6	4.8	20.7	3.6	18.1	3.11	22.3
1.25	-6.1	37.9	4.7	19.0	3.3	13.9	3.31	18.1
TOTAL	-72.2		27.3		13.3		14.73	

results from the strong outflow of M1 eastward at low levels and the strong inflowing air especially east of M1. This helps locate the gust front associated with M1 at 1845 and 1847 MDT as well as a new gust front that develops at 1850 MDT associated with the M3 (Figures 4.15, 4.16, and 4.17).

The most interesting changes for η occur within the microburst domain as maximum positive and negative η centers pivot around M1 and become oriented northwest to southeast through the center of M1 with positive η to the northwest (Fig. 4.17). The tight horizontal gradient of η values along the gust front weakens slightly with time and it appears in crossection (Fig. 4.18) that the slope of the front is most shallow at 1850 MDT in fact approaching horizontal above and southeast of M1. This is to say that negative η is being generated and is being spread out to the southeast in the lower levels of the storm. Tables 4.15 and 4.16 shows, especially in the microburst domain, that positive η is being generated above 0.75 km and destroyed below 0.75 km.

The η field in Figure 4.15 has its strongest negative value, $-32 \times 10^{-3}\ s^{-1}$, at this level (0.5 km) just east of M1. The gust front is closest to M1 at this point. The η field parallels if not defines the location of the gust front with its very tight gradient adjacent to the gust front.

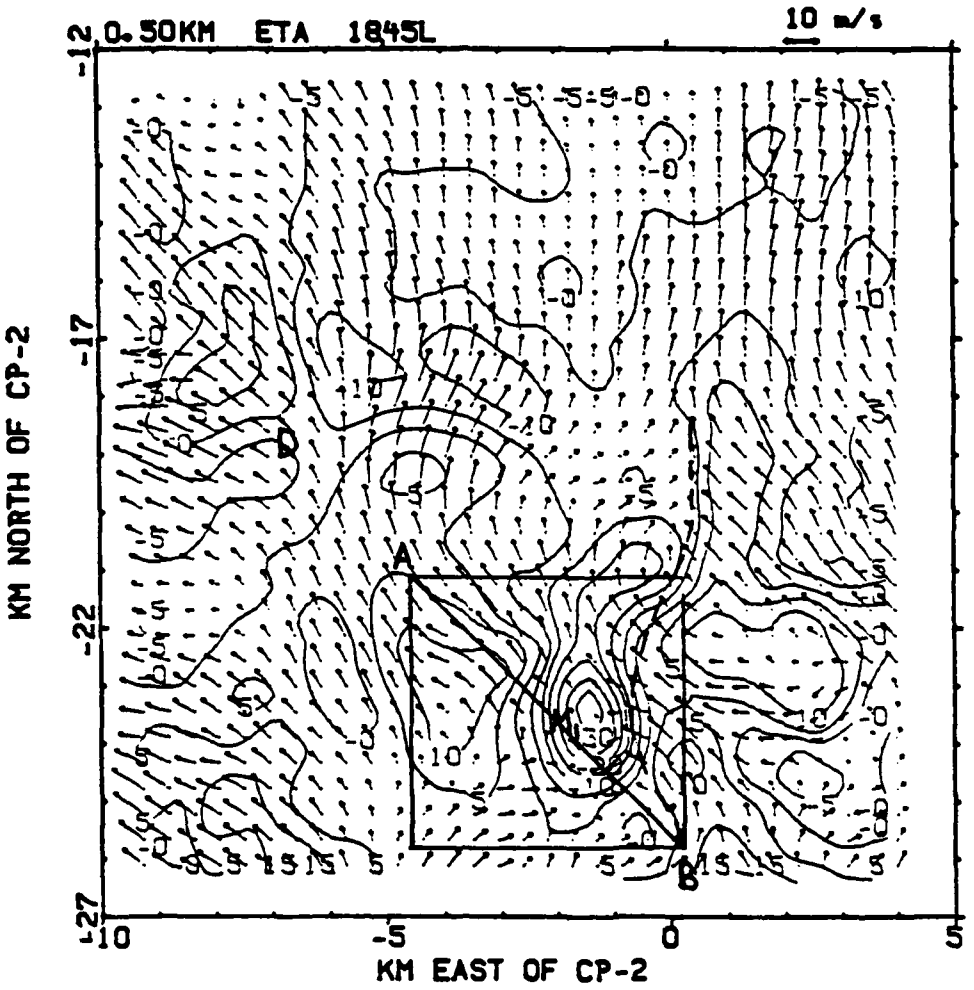

Fig. 4.15: Same as Fig. 4.9 except for η vorticity field.

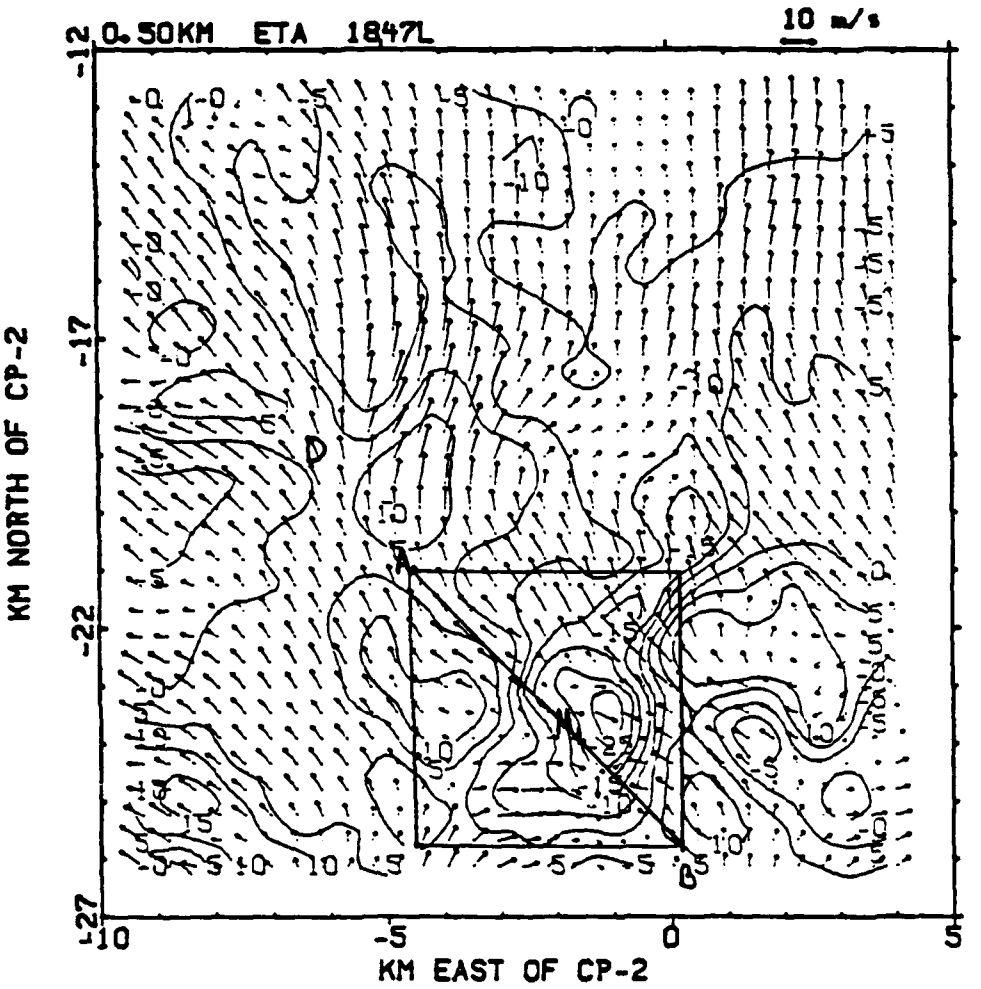

Fig. 4.16: Same as Fig. 4.11 except for η vorticity.

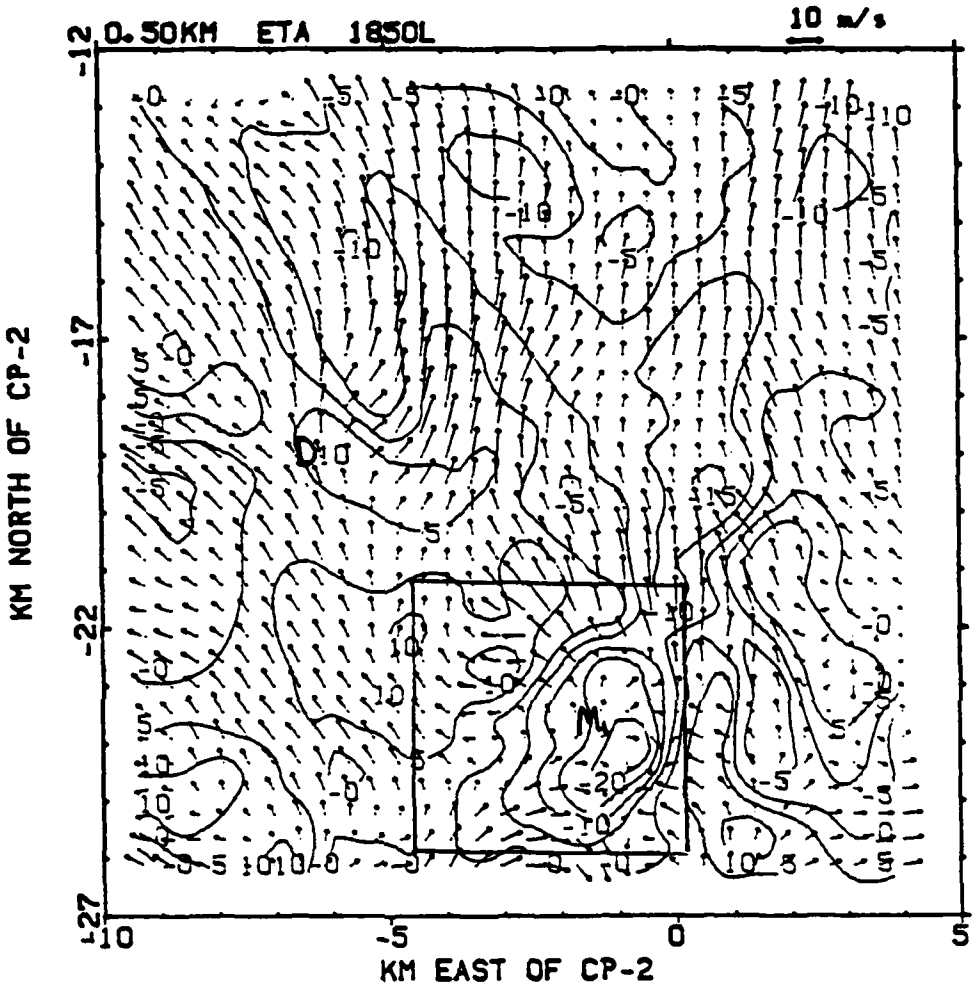

Fig. 4.17: Same as Fig. 4.12 except for η vorticity.

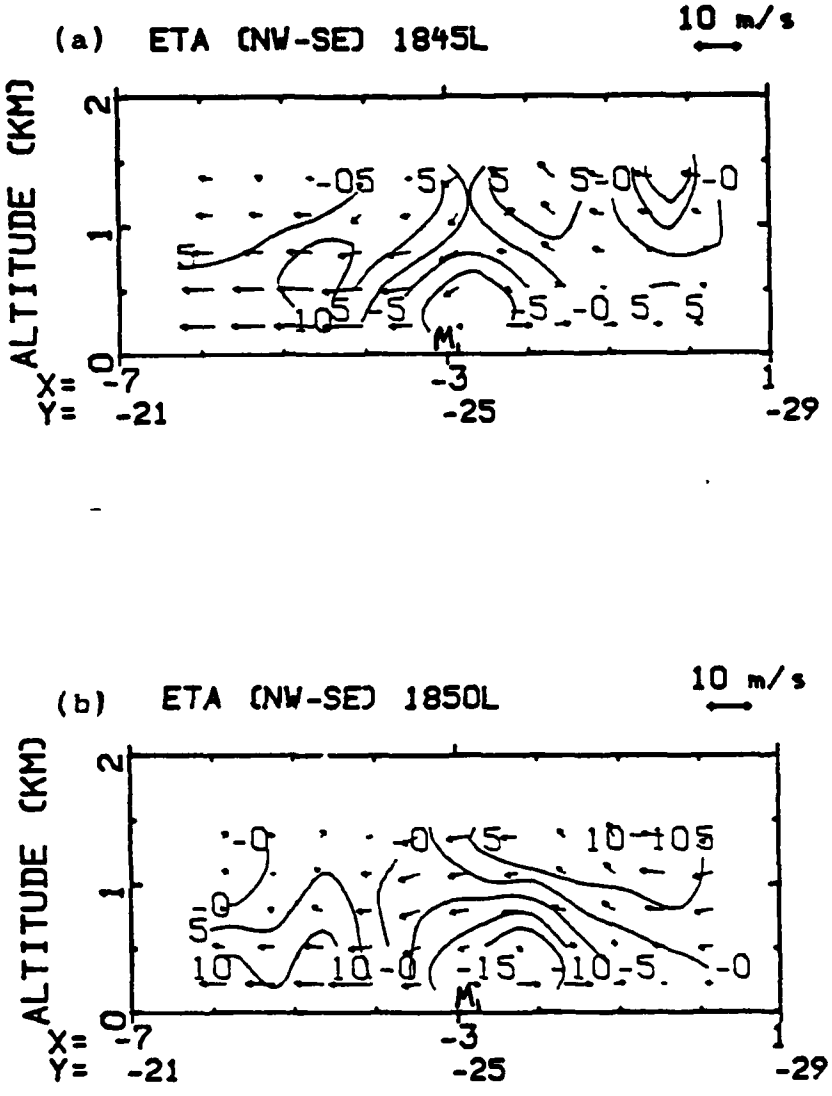

Figure 4.18: NW-SE vertical cross section of η vorticity on wind field for (a) 1845 and (b) 1850 MDT, 5 August 1982. Location of M1 is indicated.

4.3.4 η Budget

Figure 4.19 displays the vertical profile of $\langle\eta\rangle$ at the microburst domain. This change is more significant than at the storm domain. $\langle\eta\rangle$ experiences a decrease at the 1847 MDT time period. $\langle\eta\rangle$ increases again by 1850 MDT but does not exceed its initial 1847 MDT vertically averaged value. The tilting term seems to play the biggest role in making this decrease occur. Table 4.19 shows the budget terms for η. HAD and VAD and likewise, DIV and TILT act, in general, to oppose each other.

4.3.5 Z-direction Vorticity Analysis (ζ)

Figure 4.20 shows the ζ field in plan view at 0.5 km, and Tables 4.15 and 4.16 list the area means standard deviations by level for both domains. From Table 4.15, it is apparent that ζ changes very little statistically at the storm domain. The largest changes occur in the microburst domain (Fig. 4.7).

From Fig. 4.20, two areas of positive ζ are evident. One area west of M1 (area > 4×10^{-3} s^{-1}) at 0.5 km and the other along the gust front with a maximum (14×10^{-3} s^{-1}) associated with the mesocyclonic-like vortex, c_1, located at the southern end of this gust front at 1845 MDT.

By 1847 MDT (Fig. 4.21), the area along the gust front has been split as ζ is diminished just south of M1 and this continues at 1850 MDT (Fig. 4.22). The mesocyclone-like vortex, c_1, weakens with time.

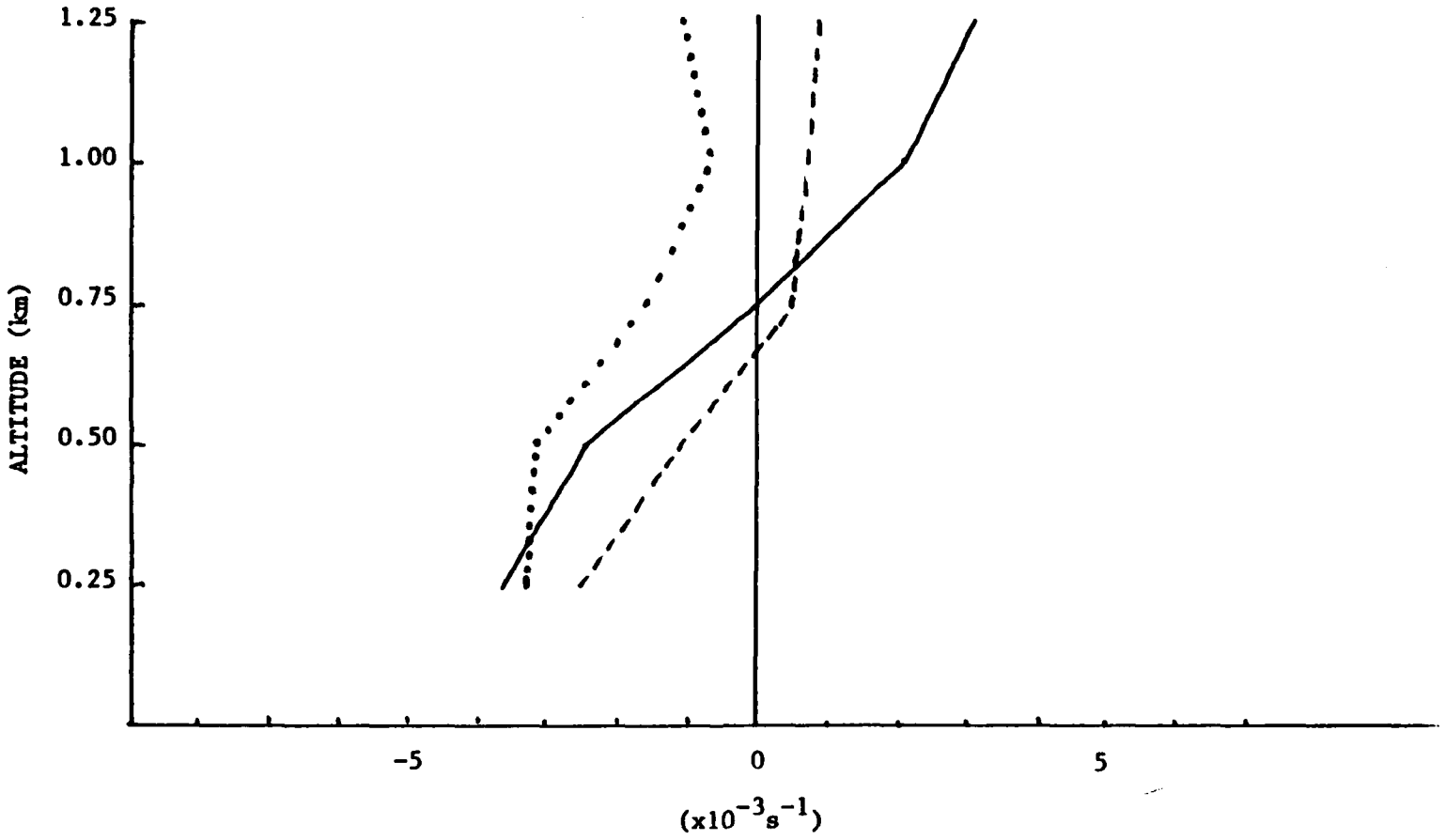

Fig. 4.19: Same as Fig. 4.14 except η vorticity is depicted.

Table 4.19: Area mean (< >) and standard deviation (σ) values for the terms of the y-component vorticity equation over the microburst domain for (a) 1845, (b) 1847, (c) 1850 MDT, 5 Aug 1982. Units are ($x10^{-6}$) s^{-2}.

(a)

Ht(km)	<HAD>	HAD_σ	<VAD>	VAD_σ	<DIV>	DIV_σ	<TILT>	$TILT_\sigma$
0.25	11.50	56.1	-0.19	4.2	-0.32	48.2	-0.23	40.1
0.50	13.90	60.5	-1.90	16.9	-2.20	14.1	1.90	30.5
0.75	9.00	53.9	-4.30	28.3	-1.80	10.2	3.60	24.4
1.00	0.82	37.6	-2.10	23.4	-0.80	12.1	3.90	22.3
1.25	-4.20	37.4	0.64	16.6	0.22	9.8	0.90	24.3
TOTAL	31.02		-7.85		-4.90		10.07	

(b)

Ht(km)	<HAD>	HAD_σ	<VAD>	VAD_σ	<DIV>	DIV_σ	<TILT>	$TILT_\sigma$
0.25	0.79	50.1	-0.25	5.7	3.5	39.2	-16.5	40.8
0.50	6.64	59.5	-0.02	18.5	1.3	27.4	-6.5	29.9
0.75	5.23	62.7	3.36	24.0	-1.8	21.0	3.7	26.9
1.00	3.75	51.6	2.71	26.9	-1.7	10.4	8.8	23.8
1.25	1.95	35.7	-0.33	27.1	-1.4	8.4	8.0	32.0
TOTAL	18.36		5.47		-0.1		-2.5	

(c)

Ht(km)	<HAD>	HAD_σ	<VAD>	VAD_σ	<DIV>	DIV_σ	<TILT>	$TILT_\sigma$
0.25	-14.30	46.5	2.00	5.2	5.10	35.7	-8.0	38.2
0.50	-9.00	44.6	6.20	18.5	5.70	22.5	-7.0	31.2
0.75	-0.41	29.8	4.70	29.8	-0.33	11.9	4.1	28.5
1.00	-0.34	26.9	-0.61	26.9	-0.25	10.3	5.3	22.3
1.25	-3.10	19.2	-0.71	19.2	1.89	9.3	3.1	20.7
TOTAL	-27.15		11.58		12.11		-2.5	

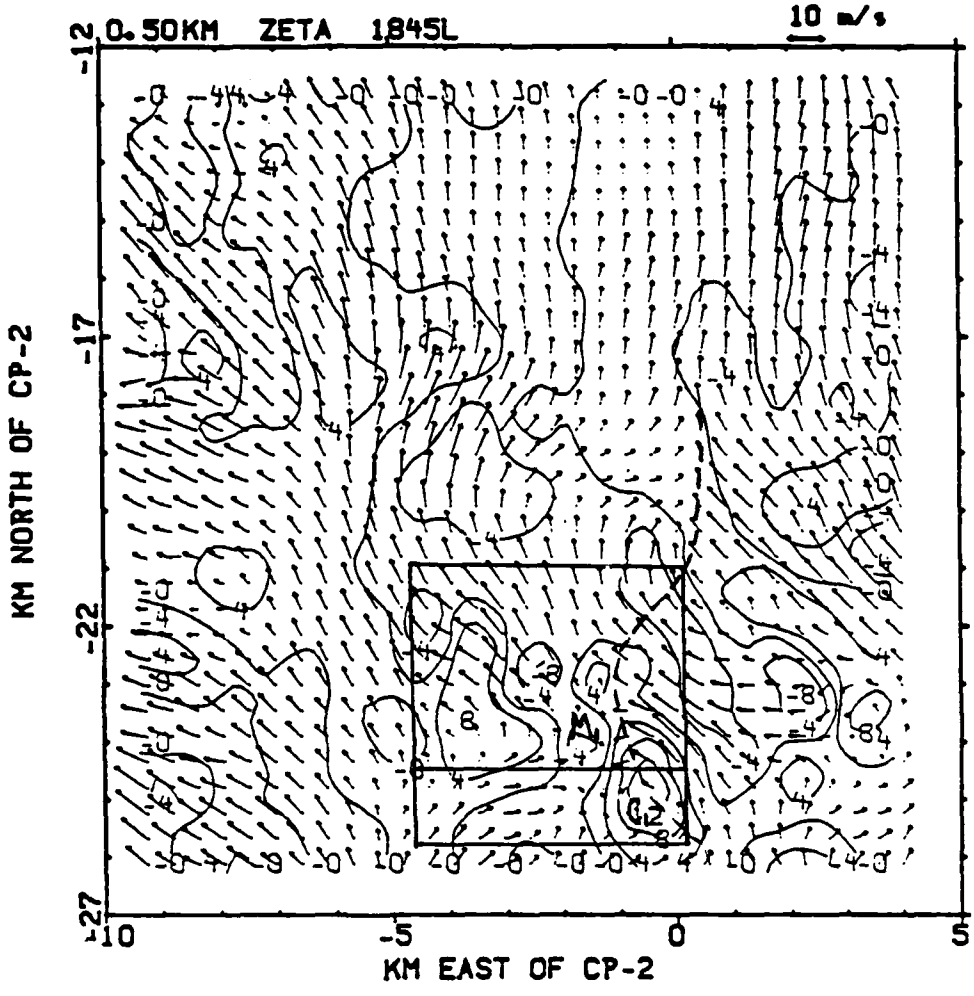

Figure 4.20: Same as Fig. 4.9 except ζ field and W-E cross section is depicted.

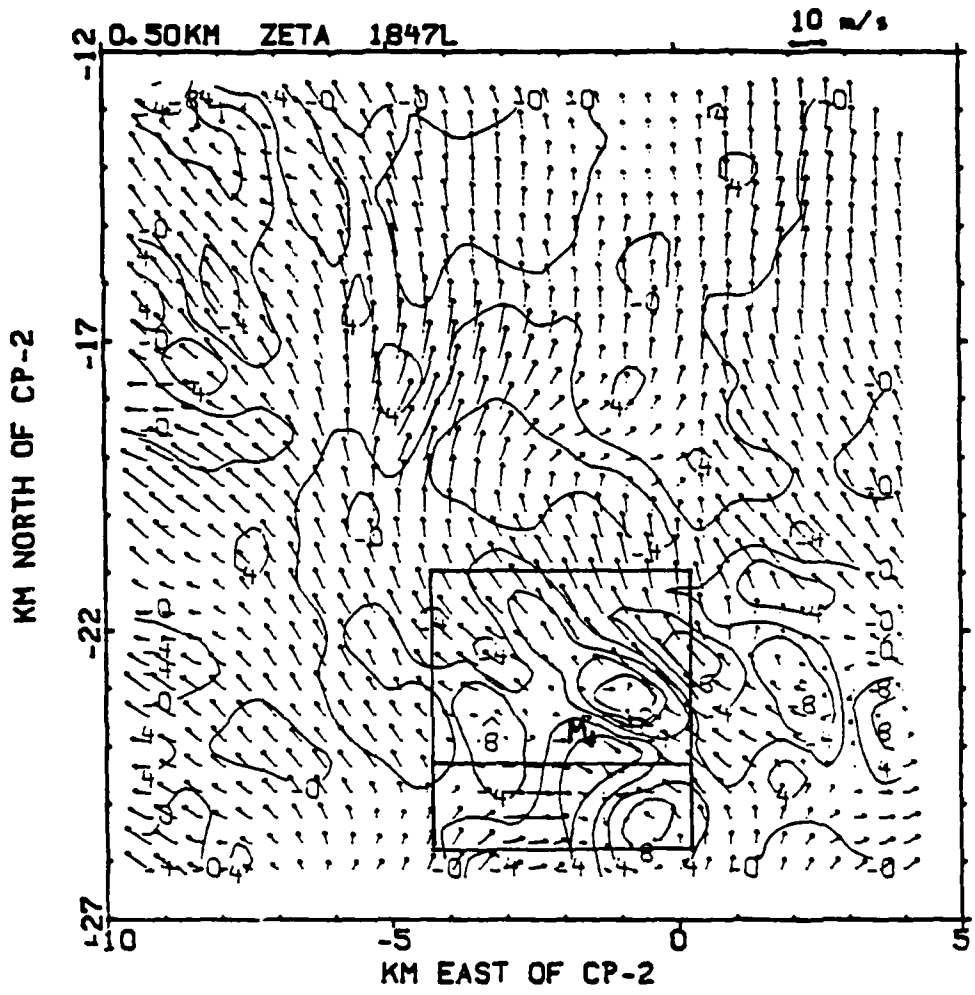

Figure 4.21: Same as Fig. 4.20 except for 1847 MDT, 5 August 1982.

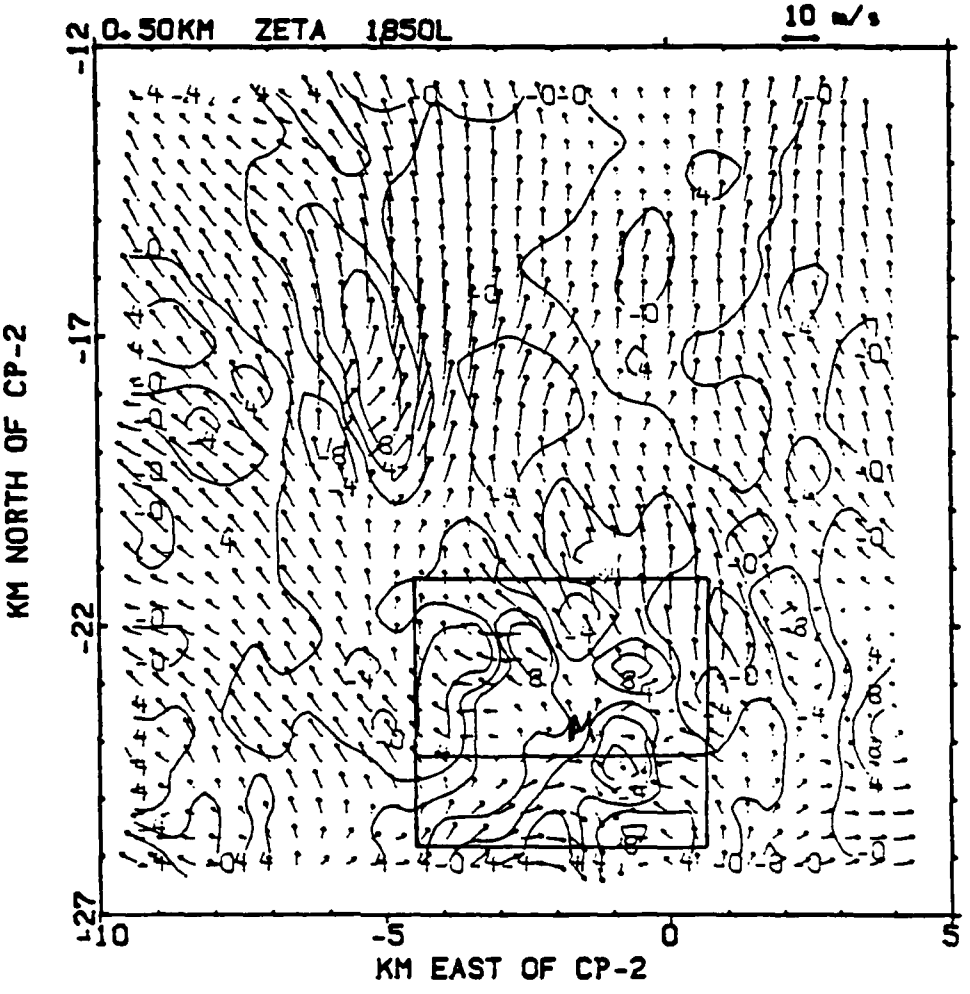

Figure 4.22: Same as Fig. 4.20 except for 1850 MDT, 5 August 1982.

The area of ζ greater than 12 x 10^{-3} s^{-1} tracks northwestward with time, weakens as it approaches M1, and merges with the positive ζ area to the west of M1.

A west-east cross section (Fig. 4.23) shows that initially the area west of M1 is shallow extending only up to 0.5 km. By 1847 MDT and continuing at 1850 MDT, this area experiences a spin up of vorticity from the top down. A new misocyclone, c2, develops here by 1850 MDT with maximum ζ vorticity occuring at 1.25 km of 14 x 10^{-3} s^{-1}.

ζ is a maximum, 14 x 10^{-3} s^{-1}, in the mesocyclone-like vortex and is positive along the gust front. Another region of postive ζ values is located west of M1. The W-E cross section through the microburst domain in Figure 4.23a indicates the positive area west of M1 is a low level feature while the area along the gust front extends through several levels and slopes westward with height, i.e., with the updraft in this area. In the column directly above M1, ζ is negative below 0.75 km and positive above although the values are relatively small, i.e., near zero throughout. This signifies that the flow is largely irrotational through the horizontal plane.

Table 4.15 lists the area mean and standard deviation values for each component of vorticity by level for the storm domain. By comparing area mean values of ξ, η, and ζ, it is seen that ξ and ζ are the predominantly positive over the storm domain with the strongest values above 0.5 km. η values have negative values at the lower levels, 0.25 km and 0.5 km.

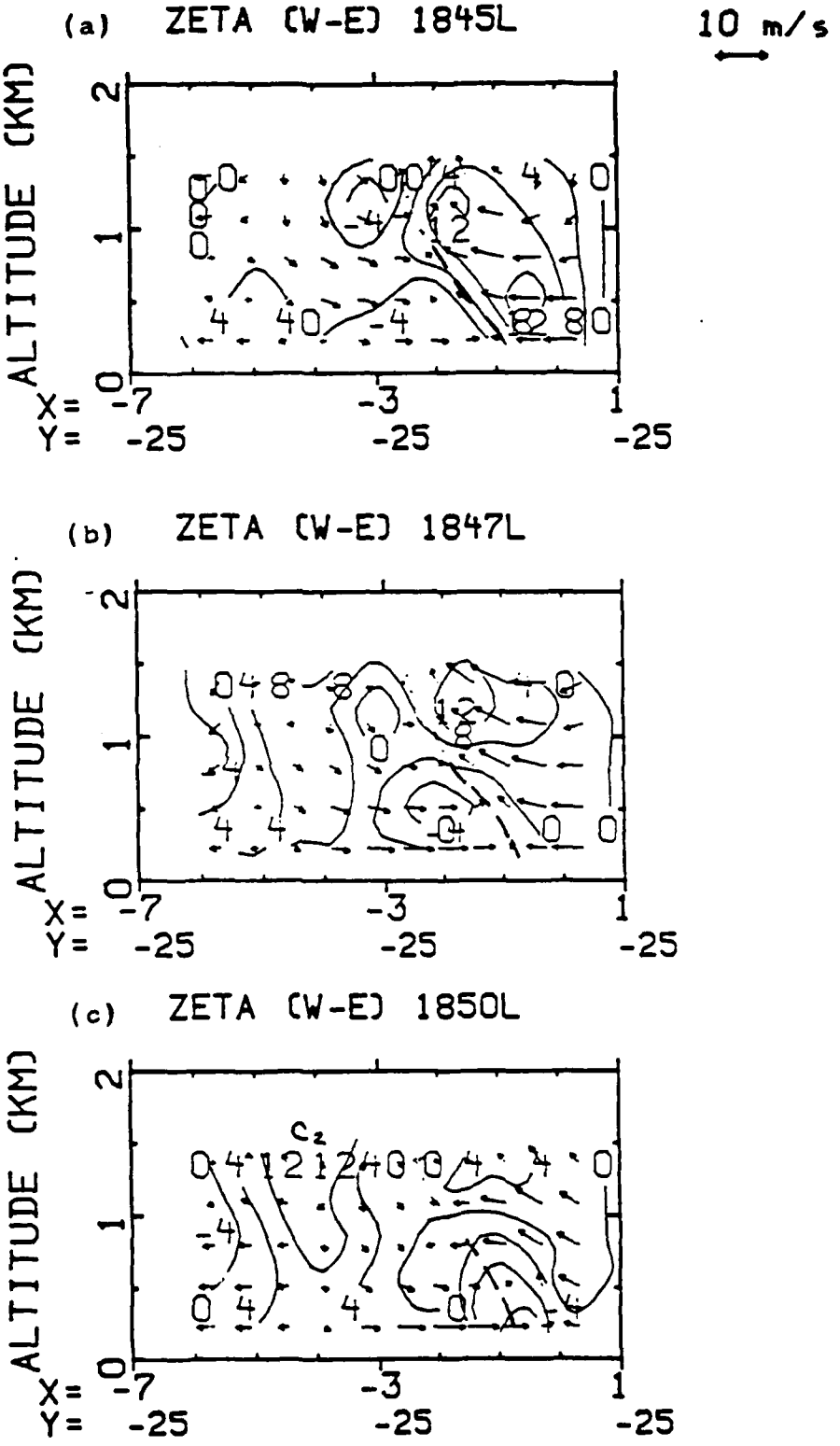

Figure 4.23: W-E cross section of ζ vorticity at (a) 1845, (b) 1847, and (c) 1850 MDT, 5 August 1982. Gust front is indicated by dashed line.

In the microburst domain (Table 4.16), ξ and η are predominantly negative in the mean below 0.75 km (ξ) and 0.5 km (η) while ζ continues to be postive throughout with the larger mean values at the higher levels of the microburst domain.

4.3.6 ζ Budget

The ζ budget terms in the storm domain for virtually all times were found to be less than those in the microburst domain. Area mean values were typically on the order of 1×10^{-7} s^{-2} in the storm domain and 1×10^{-6} s^{-2} in the microburst domain indicating the many more complex and opposing interactions at the storm domain. Typical values, while being of the same order in both domains were larger in the microburst domain and extended through more depth.

The microburst domain ζ budget terms are presented in Table 4.20 for all analysis times. The last row is a vertical sum of the area means of each term. This provides a look at which terms act as a source or sink for ζ. It can be seen that DIV and TILT become important, especially at 1847 and 1850 MDT at 0.75 to 1.25 km. Both of these terms act positively to generate ζ. So it appears that the contribution from DIV is critical to the formation and development of the misocyclone.

Figure 4.24 shows a vertical profile of area means for ζ at each analysis time for the microburst domain. The $\langle\zeta\rangle$ field experiences virtually no change with time while maintaining a net positive component at all levels.

Table 4.20: Area mean (< >) and standard deviation (σ) values of the terms of the z-component vorticity equation over the microburst domain for (a) 1845, (b) 1847, and (c) 1850 MDT, 5 Aug 1982. Units are ($x10^{-6}$) s^{-2}.

(a)

Ht(km)	<HAD>	HAD_σ	<VAD>	VAD_σ	<DIV>	DIV_σ	<TILT>	$TILT_\sigma$
0.25	-1.80	28.6	0.23	3.4	4.90	14.4	1.80	9.4
0.50	2.80	30.3	1.5	8.5	-0.03	7.9	-0.85	11.6
0.75	1.90	26.9	1.99	15.2	-0.30	8.4	-2.10	13.9
1.00	0.54	28.6	2.1	11.2	0.36	10.1	-1.30	15.4
1.25	-1.90	24.1	2.1	22.7	1.70	7.0	-0.83	24.8
TOTAL	1.54		7.92		6.63		-3.28	

(b)

Ht(km)	<HAD>	HAD_σ	<VAD>	VAD_σ	<DIV>	DIV_σ	<TILT>	$TILT_\sigma$
0.25	4.90	36.8	-0.13	3.9	-0.75	16.5	-1.9	12.6
0.50	5.70	27.0	-0.58	9.4	-2.26	9.1	-1.6	16.4
0.75	0.92	30.9	-2.61	13.9	0.16	9.5	1.9	16.6
1.00	-4.75	27.9	-1.58	10.5	2.67	10.3	4.5	13.3
1.25	-6.50	26.1	0.45	14.4	4.00	9.3	4.6	16.2
TOTAL	0.27		-4.45		3.82		7.5	

(c)

Ht(km)	<HAD>	HAD_σ	<VAD>	VAD_σ	<DIV>	DIV_σ	<TILT>	$TILT_\sigma$
0.25	8.39	34.5	-0.11	4.89	-4.40	15.8	-3.1	11.1
0.50	4.94	38.2	-1.46	10.20	-1.70	11.4	-1.3	14.5
0.75	-0.06	32.9	-2.91	13.30	-0.84	7.6	2.4	12.5
1.00	-4.76	21.6	0.22	12.50	2.41	8.0	1.6	15.5
1.25	-5.50	15.4	3.62	14.40	3.38	6.3	-1.5	19.0
TOTAL	3.01		-0.64		-1.15		-1.9	

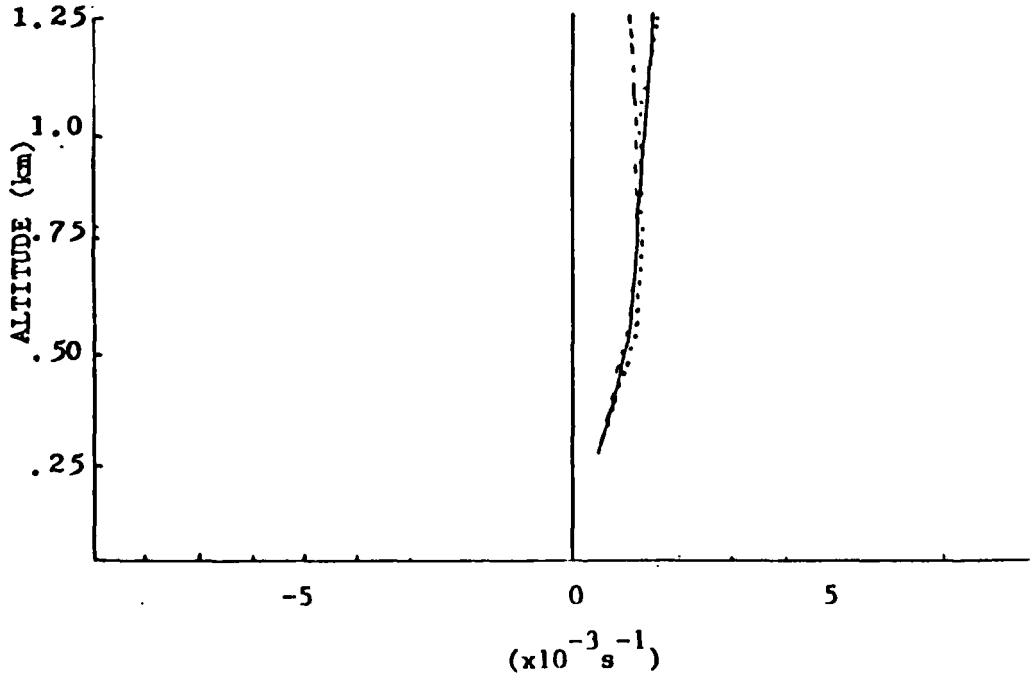

Fig. 4.24: Same as Fig. 4.14 except ζ vorticity is depicted.

5. Conclusions

Horizontal vorticity maxima/minima were found in regions of strong horizontal gradients of vertical velocity above the lowest layers. In the lower layers, but outside the immediate center of the microburst, these horizontal vorticity centers were enhanced by the vertical shear of the horizontal winds.

Vertical vorticity, ζ, was positive above about 1 km for the 14 July 1982, simple case and virtually zero or negative below. The microburst flow, then, appeared to be irrotational.

Similar results for the complex case were found. The 5 August case had a stronger environmental flow. Its microburst, M_1, was less downward directed, but rather, directed outward (to the north) and down. The horizontal gradient of vertical velocity suffered in strength due to these features. The horizontal components are maximized along the gust front where convergence is important and when M_1 begins to decay and its outflow is teamed with that of M_3.

The simple case of 14 July 1982 illustrated the existence of a vortex ring, envisioned by Fujita (1985), surrounding the microburst downflow. This ring descended from 0.75 km at 1647 MDT to 0.5 km at 1649 MDT. The effect was to create increased surface winds SW and NE (along the gust fronts) as the ring descended. The increased surface winds and the development or reformation of the gust front at 1649 MDT led to the increased

significance of the divergence term in creating positive and negative valued horizontal vorticity areas. That is, the increased surface winds create a larger vertical wind shear which implies larger horizontal vorticity components.

The vortex ring and rotor does have low perturbation pressure associated with it as Kessinger *et al.* (1988) found with their actual pressure measurements via a PAM and their pressure perturbation analysis. The low pressure has been deemed responsible for accelerating the surface winds as has been mentioned. The derived perturbation pressure field describes the necessary pressure gradient to account for the wind field. The existence of the vortex ring explains the location of the low pressure and maximum surface winds. Finally, it was shown that the overall vorticity vector was quasi-horizontal in this case. The z-direction vorticity budget illustrated the opposing nature of the vertical advection and tilting terms. Hence, ζ was destroyed through the tilting term as vertical advection attempted to build ζ from the top down.

The complex case of 5 August 1982 showed the evolution of the misocyclone. It was seen that the positive ζ was generated from the top down as Kessinger *et al.* (1988) and Ray *et al.* (1975) also suggested. The lack of sufficient convergence in the low-levels of the storm perhaps destroyed the opportunity for the first circulation along the gust front to spin up. Another possible explanation is that M_1's diverging flow served to lessen the existing positive vertical vorticity, ζ, in low-

levels as witnessed by the disappearance of the mesocyclone-like vortex, c_1. As the diverging flow continued, c_1 weakened and disappeared. The opposing flow of M_1 towards the south is not strong and does not allow sufficient convergence.

Further, ζ (positive values) sloped westward over the microburst with height and allowed the VAD term to act as a source. While the TILT term acted as a sink at 1845 MDT, it began to generate ζ at the higher levels at 1847 and 1850 MDT. The final contribution from the DIV term, acting strongly positive particularly at 1847 and 1850 MDT, allowed the spin up of ζ to continue with the misocyclone, c_2, resulting.

Vorticity budget analyses were also conducted for each direction for each case. The magnitude of the budget terms over the microburst domain have been shown to be larger than those over the larger storm domain. Hence, the existence of the microburst enhances the magnitude of the vorticity components in the near microburst region of the storm. This was true for both cases and for each component of vorticity.

Lastly, some measure of comparison between the cases should be mentioned. All three components of vorticity are stronger in a root mean square comparison in the 5 August case at the microburst domain. The stronger inflowing environmental air allowed for greater vertical shear and larger horizontal vorticity components.

In a budget sense and since the components were larger in the 5 August case, the budget terms should be larger for the 5

August case than for the 14 July case. This was found to be true with special notice to the considerably larger DIV term in the 5 August case, especially in the z-direction. It is believed that this term contributed greatly to the development of the misocyclone.

There were no apparent consistent sources or sinks between cases. That is, for example, if the tilting term was a source for one component at one time, it was not necessarily a source at a later time or for a subsequent case.

Further study is needed to determine why the rotors develop in some cases and not in others. It may be a combination of convergence and opposing flow. That is, for the 14 July case, the rotor did not form south of the microburst where the divergence magnitude (-12×10^{-3} s^{-1}) is the same as in the north where the rotor did form. Therefore, convergence alone is not enough, but the flow in the north was opposing the environment which may be of consequence. Also with sufficient time resolution, the propagation of these vortices and rotors may be studied. The solenoidal term, although believed to be small, may contribute in the head of the gust front. This may be important in the formation of the rotor. The elongated region of horizontal vorticity mentioned for the 5 August case also coincides with a perturbation temperature gradient. Perhaps, this is a hint of possible solenoidal activity.

APPENDIX

1. Vorticity Equations: By taking the curl ($\nabla\times$) of the equation of motion in vector form, the following vorticity equation results:

$$d\vec{q}_a/dt = -\vec{q}_a(\vec{\nabla}\cdot\vec{V}) + \vec{q}_a\cdot\vec{\nabla}\vec{V} - \vec{\nabla}\times(\alpha\vec{\nabla}P) + \vec{\nabla}\times\vec{F}$$

where $\vec{V}$ is the three dimensional wind vector;

$\vec{q}_a = \vec{q} + 2\vec{\Omega}$, is the absolute vorticity vector;

$d/dt = \partial/\partial t + \vec{V}_h\cdot\vec{\nabla}_h + w\partial/\partial z$, is the total derivative;

$\vec{\nabla} = \vec{\nabla}_h + \hat{k}\partial/\partial z$, is the 3-D del operator;

$\vec{q} = \hat{i}\xi + \hat{j}\eta + \hat{k}\zeta$, is the relative vorticity vector;

$2\vec{\Omega} = \hat{i}0 + \hat{j}\,2\Omega\cos\phi + \hat{k}\,2\Omega\sin\phi$, is the angular velocity vector of the earth, $\hat{i}$, $\hat{j}$, and $\hat{k}$ are unit vectors toward the x-, y-, and z-axes, respectively.

Equation (1) is the complete form of the vorticity equation in Cartesian coordinates in the relative frame of reference. Where (1) is applied to the convective scale motion, such as, the meso-β scale (Orlanski, 1975), the contribution due to the earth's rotation to the absolute vorticity, 2Ω, becomes sufficiently small. Hence $\vec{q}_a$ can be replaced by $\vec{q}$. It follows that (1) can be rewritten as:

$$dq/dt = \partial q/\partial t + \vec{V}\cdot\vec{\nabla}q + w\partial q/\partial z$$
$$= -q(\vec{\nabla}_h\cdot\vec{V}_h + \partial w/\partial z) + \vec{q}\cdot\vec{\nabla}\vec{V} - \vec{\nabla}\times(\alpha\vec{\nabla}P) + \vec{\nabla}\times\vec{F}$$

where term A is the local time rate of change of the relative vorticity vector;

term B is the horizontal advection of q;

term C is the vertical advection of q;

term D is the divergence term;

term E is the tilting term;

term F is the solenoid term;

and term G is the friction term.

Term D can be expanded as:

$$D: \quad -(\hat{i}\xi + \hat{j}\eta + \hat{k}\zeta)(\partial u/\partial x + \partial v/\partial y + \partial w/\partial z) \quad (3)$$

Similarly, terms E, F, and G can also be expanded as:

$$E: \quad ((\hat{i}\xi + \hat{j}\eta + \hat{k}\zeta)\cdot\nabla)(\hat{i}u + \hat{j}v + \hat{k}w) \quad (4)$$

$$F: \quad -\vec{\nabla} \times (\alpha\vec{\nabla}P) = -\vec{\nabla}\alpha \times \vec{\nabla}P = -\hat{i}(\partial\alpha/\partial y\partial p/\partial z - \partial\alpha/\partial z\partial p/\partial y) \quad (5)$$
$$+ \hat{j}(\partial\alpha/\partial z\partial p/\partial x - \partial\alpha/\partial x\partial p/\partial z) - \hat{k}(\partial\alpha/\partial x\partial p/\partial y - \partial\alpha/\partial y\partial p/\partial x)$$

$$G: \quad (\hat{i}\partial/\partial x + \hat{j}\partial/\partial y + \hat{k}\partial/\partial z) \times (\hat{i}F_x + \hat{j}F_y + \hat{k}F_z) = \quad (6)$$
$$\hat{i}(\partial F_z/\partial y - \partial_y/\partial z) + \hat{j}(\partial F_x/\partial z - \partial F_z/\partial x) + \hat{k}(\partial F_y/\partial x - \partial F_x/\partial y)$$

Remember, the vorticity equation, thus far, has been operated in the coordinate system with respect to the earth.

In a convective storm with a constant translational speed, c, it is essential to use the storm-relative coordinate system or rather, moving coordinates with the system's origin at the center of the storm. This is particularly needed in a thermodynamical retrieval study. Recall, the velocity vector, V, is the total wind vector, including both the storm-relative wind vector, $\vec{V}_r$, and the storm motion, c, i.e.,

$$\vec{V} = \vec{V}_r + \vec{c} \qquad (7)$$

If the storm motion is nearly stationary, c≈0, then

$$V \approx V_r \qquad (8)$$

For the storm cases under investigation using the JAWS data, c is very small, therefore, no space-time conversion is needed. In other words, V can be treated as V_r, etc. However, if the system is moving, the storm-relative wind vector, V_r, must be used to replace V. Remember,

$$\vec{\nabla}\cdot\vec{V} = \vec{\nabla}\cdot(\vec{V}_r + \vec{c}) = \vec{\nabla}\cdot\vec{V}_r + \cancel{\vec{\nabla}\cdot\vec{c}}^{\,0}$$

$$\vec{\nabla} \times \vec{V} = \vec{\nabla} \times (\vec{V}_r + \vec{c}) = \cancel{\vec{\nabla} \times \vec{c}}^{\,0} + \vec{\nabla} \times \vec{V}_r \qquad (9)$$

$$\partial u/\partial x = \partial/\partial x\,(u_r + c_x) = \partial u_r/\partial x + \cancel{\partial c_x/\partial x}^{\,0} = \partial u_r/\partial x$$

and so forth.

From now on, V can be thought of as V_r; however, for convenience, the subscript r will be dropped. Furthermore, the friction term, in general, is one order of magnitude smaller then the other terms in (2) and will be dropped hereafter.

2. Vorticity components in moving coordinates (x,y,z): Three vorticity component equations in moving coordinates (x,y,z,t) can be derived from (2) by performing dot (i,j,and k) products on (2). This yields:

$$\partial\xi/\partial t = -\vec{V}_h \cdot \vec{\nabla}_h \xi - w\partial\xi/\partial z - \xi(\vec{\nabla}_h \cdot \vec{V}_h + \partial w/\partial z) + (\xi\partial u/\partial x + \eta\partial u/\partial y + \zeta\partial u/\partial z) - (\partial\alpha/\partial y\partial p/\partial z - \partial\alpha/\partial z\partial p/\partial y)$$

$$\partial\eta/\partial t = -\vec{V}_h \cdot \vec{\nabla}_h \eta - w\partial\eta/\partial z - \eta(\vec{\nabla}_h \cdot \vec{V}_h + \partial w/\partial z) + (\xi\partial v/\partial x + \eta\partial v/\partial y + \zeta\partial v/\partial z) - (\partial\alpha/\partial z\partial p/\partial x - \partial\alpha/\partial x\partial p/\partial z) \quad (10)$$

$$\partial\zeta/\partial t = -\vec{V}_h \cdot \vec{\nabla}_h \zeta - w\partial\zeta/\partial z - \zeta(\vec{\nabla}_h \cdot \vec{V}_h + \partial w/dz) + (\xi\partial w/\partial x + \eta\partial w/\partial y + \zeta\partial w/\partial z) - (\partial\alpha/\partial x\partial p/\partial y - \partial\alpha/\partial y\partial p/\partial x)$$

where $\xi = \partial w/\partial y - \partial v/\partial z$ is the vorticity component about the x-axis;

$\eta = \partial u/\partial z - \partial w/\partial x$ is the vorticity component about the y-axis; and

$\zeta = \partial v/\partial x - \partial u/\partial y$ is the vorticity component about the z-axis.

3. Computation of vorticity budgets: Equation (10) can be used to compute te vorticity generation of a mesoscale system, e.g., the mesocyclone, the microburst misocyclone, etc. Excepting the solenoidal term, which uses the information from the Doppler derived wind field and is subject to larger uncertainty, the other terms can be determined from the three wind

components (u,v,w) and their derivatives.

REFERENCES

Armijo, L., 1969: A Theory for the Determination of Wind and Precipitation Velocities with Doppler Radars. *J. Atm. Sci.*, *26*, 570-574.

Blechman, J. B., 1980: Vortex Generation in a Numerical Thunderstorm Model. *Monthly Weather Review*, *109*, 1061-1071.

Coover, J. A. Jr., 1988: Kinematic and Dynamic Studies of Microbursts in the Sub-Cloud Layer Derived From JAWS Dual-Doppler Radar for a Colorado Thunderstorm. Ph.D. Dissertation, St. Louis University, 225pp.

Fujita, T. T., 1985: *The Downburst Microburst and Macroburst*. University of Chicago Press, 122 pp.

Fujita, T. T., 1986: DFW Microburst on August 2, 1985. Satellite and Mesometeorology Research Project, Research Paper No.217, University of Chicago, 150 pp.

Gal-Chen, T., 1978: A Method for the Initialization of the Anelastic Equations: Implications For Matching Models with Observations. *Monthly Weather Review*, *106*, 587-606.

Hjelmfelt, M. R., 1987: Structure and Life Cycle of Microburst Outflows Observed in Colorado. *Journal of Applied Meteorology*, *27*, 900-926.

Johnson, K. W., P. S. Ray, B. C. Johnson, and R. P.Davies-Jones,1987: Observations Related to the Rotational Dynamics of the 20 May 1977 Tornadic Storms. *Monthly Weather Review*, *115*, 2463-2478.

Kessinger, C. J., J. W. Wilson, M. Weisman, and J. Klemp, 1984: The Evolution of Misoscale Circulations In A Downburst-Producing Storm and Comparison to Numerical Results. *22nd Conference On Radar Meteorology*, 10-13 Sept. 1984, Amer. Meteor. Soc., Boston, MA. pp. 58-63.

Kessinger, C. J., D. B. Parsons, and J. W. Wilson, 1988:Observations of a Storm Containing Misocyclones, Downbursts, and Horizontal Vortex Circulations. *Monthly Weather Review*, *116*, 1959-1982.

Klemp, J. B., and R. Rotunno, 1982: A Study of the Tornadic Region within a Supercell Thunderstorm. *J. Atm. Sci.*, *40*, 359-377.

Lin, Y. J., and P. T. Chang, 1975: Some Effects of the Shearing and Veering Environmental Wind on the Internal Dynamics and Structure of a Mature Severe Thunderstorm. Severe Storms Project, St. Louis University, St. Louis MO.

Lin, Y. J., and P. M. Condray, 1988: Momentum Flux in the Subcloud Layer of a Microburst-Producing Thunderstorm Determined from JAWS Dual-Doppler Measurements. *Boundary Layer Meteorology*, *43*, 125-141.

Lin, Y. J., and J. A. Coover, 1988: A Kinetic Energy Analysis of a Microburst- Thunderstorm Based on JAWS Dual-Doppler Data. *J. Atm. Sci.*, *45*, 2764-2771.

Lin, Y. J., and R. G. Hughes, 1987: Structural Features of a Microburst- Producing Storm in Colorado Revealed By JAWS Dual-Doppler Radars. *J. Atm. Sci.*, *44*, 3540-3655.

Lin, Y. J., R. G. Hughes, and R. W. Pasken, 1987: Subcloud-Layer Kinematic and Dynamic Structures of a Microburst-Producing Thunderstorm in Colorado Determined from JAWS Dual-Doppler Measurements. *Boundary Layer Meteorology*, *39*, 67-86.

Linden, P. F., and J. E. Simpson, 1985: Microbursts: a hazard for aircraft. *Nature*, *317*, 601-602.

McCarthy, J., R. Roberts, and W. Schreiber, 1983: JAWS Data Collection, Analysis Highlights, and Microburst Statistics. *Preprints, 21st Conf. on Radar Meteor.*, Edmonton, Alta., Canada, Amer. Meteor. Soc., 624-629.

Orlanski, I., 1975: A Rational Subdivision of Scales for Atmospheric Processes. *Bull. Amer. Meteor. Soc.*, *56*, 527-530.

Waranauskas, B. R., 1985: The Rotor Microburst: A New Explanation For Burst Swath Damage. *Preprints, 14th Conference On Severe Local Storms*, Indianapolis, Amer. Meteor. Soc., 260-263.

Wilson, J. W., R. D. Roberts, C. Kessinger, and J. McCarthy, 1984: Microburst Wind Structure and Evaluation of Doppler Radar For Airport Wind Shear Detection. *J. Climate and Appl. Meteor.*, *23*, 898-915.

BIOGRAPHY OF THE AUTHOR

Paul Gerard Lapointe [redacted] and, in 1977, he graduated from Andover High School. The author developed an interest in meteorology while studying to obtain a private pilot's license. This led him to attend the University of Lowell, in Lowell, Massachusetts where on 23 May 1981, the author was awarded his Bachelor of Science, Meteorology and was commissioned a Second Lieutenant, United States Air Force.

After serving two years as a weather forecaster at Loring Air Force Base, Maine, the author was reassigned to Offutt AFB, Omaha, Nebraska as a forecaster for the Strategic Air Command. In 1985, he was called to serve as the Executive Assistant to the Commander, Air Weather Service in an administrative capacity before being reassigned to Saint Louis University in 1987 through the Air Force Institute of Technology (AFIT).